

UC Irvine

UC Irvine Previously Published Works

Title

Dissecting Fission Yeast Shelterin Interactions via MICro-MS Links Disruption of Shelterin Bridge to Tumorigenesis

Permalink

<https://escholarship.org/uc/item/29z7t7j8>

Journal

Cell Reports, 12(12)

Authors

Liu, J

Yu, C

Hu, X

et al.

Publication Date

2015-09-29

DOI

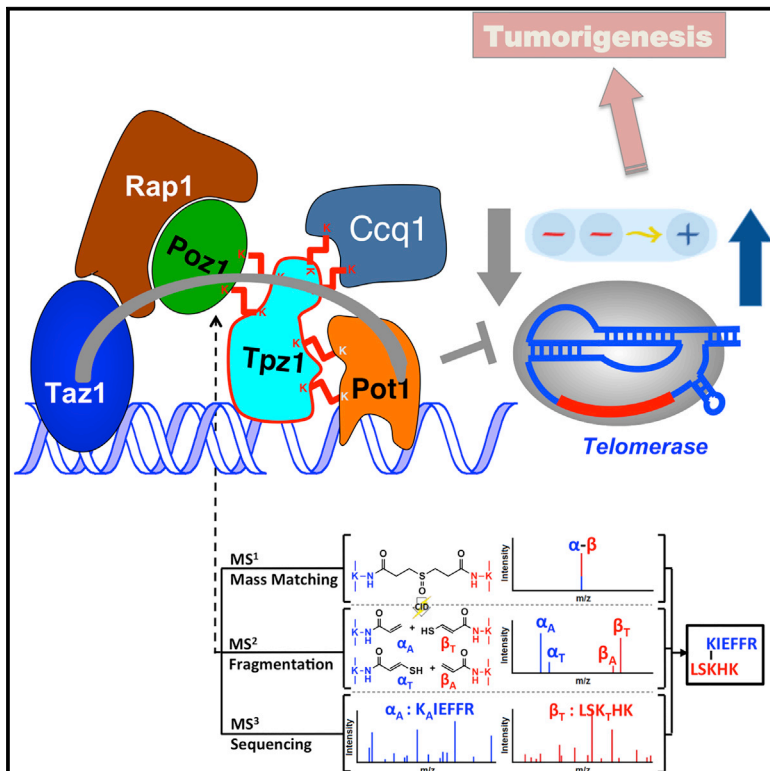
10.1016/j.celrep.2015.08.043

Peer reviewed

Cell Reports

Dissecting Fission Yeast Shelterin Interactions via MICro-MS Links Disruption of Shelterin Bridge to Tumorigenesis

Graphical Abstract



Authors

Jinqiang Liu, Clinton Yu, Xichan Hu, ..., Scott D. Rychnovsky, Lan Huang, Feng Qiao

Correspondence

qiao@uci.edu

In Brief

Liu et al. develop a strategy that identifies contact sites within a complex without a 3D structure. Using this strategy, they dissect interactions among fission yeast shelterin components and find that failure to maintain an intact human shelterin bridge leads to tumorigenesis.

Highlights

- MICro-MS can identify contact residues in protein interaction interfaces
- MICro-MS allows dissection of Tpz1-centered shelterin interfaces in fission yeast
- A POT1 variant in melanoma weakens shelterin interaction between POT1 and TPP1



Dissecting Fission Yeast Shelterin Interactions via MICro-MS Links Disruption of Shelterin Bridge to Tumorigenesis

Jinqiang Liu,¹ Clinton Yu,² Xichan Hu,¹ Jin-Kwang Kim,¹ Jan C. Bierma,¹ Hyun-Ik Jun,¹ Scott D. Rychnovsky,³ Lan Huang,² and Feng Qiao^{1,*}

¹Department of Biological Chemistry, School of Medicine, University of California, Irvine, Irvine, CA 92697-1700, USA

²Department of Physiology and Biophysics, School of Medicine, University of California, Irvine, Irvine, CA 92697-4560, USA

³Department of Chemistry, University of California, Irvine, Irvine, CA 92697-2025, USA

*Correspondence: qiao@uci.edu

<http://dx.doi.org/10.1016/j.celrep.2015.08.043>

This is an open access article under the CC BY-NC-ND license (<http://creativecommons.org/licenses/by-nc-nd/4.0/>).

SUMMARY

Shelterin, a six-member complex, protects telomeres from nucleolytic attack and regulates their elongation by telomerase. Here, we have developed a strategy, called MICro-MS (Mapping Interfaces via Crosslinking-Mass Spectrometry), that combines crosslinking-mass spectrometry and phylogenetic analysis to identify contact sites within the complex. This strategy allowed identification of separation-of-function mutants of fission yeast Ccq1, Poz1, and Pot1 that selectively disrupt their respective interactions with Tpz1. The various telomere dysregulation phenotypes observed in these mutants further emphasize the critical regulatory roles of Tpz1-centered shelterin interactions in telomere homeostasis. Furthermore, the conservation between fission yeast Tpz1-Pot1 and human TPP1-POT1 interactions led us to map a human melanoma-associated POT1 mutation (A532P) to the TPP1-POT1 interface. Diminished TPP1-POT1 interaction caused by hPOT1-A532P may enable unregulated telomere extension, which, in turn, helps cancer cells to achieve replicative immortality. Therefore, our study reveals a connection between shelterin connectivity and tumorigenicity.

INTRODUCTION

The six-member telomere shelterin complex is vital for eukaryotic cells. It functions to regulate telomere elongation by telomerase, as well as to protect the ends of linear chromosomes from degradation and recognition as DNA damage sites (Artandi and Cooper, 2009; Jain and Cooper, 2010; Palm and de Lange, 2008). In human cells, the shelterin complex consists of double-stranded DNA (dsDNA) binders TRF1 and TRF2, single-stranded DNA (ssDNA) binder POT1, as well as RAP1, TIN2, and TPP1 (de Lange, 2005). The shelterin connects telomeric

dsDNA with ssDNA by forming a proteinaceous bridge via protein interactions within the shelterin. Specifically, telomeric dsDNA binders TRF1 and TRF2 recruit TIN2 and RAP1 to the telomere; TIN2 then recruits TPP1-POT1 complex to the telomere (Takai et al., 2011). Since POT1 directly binds to the telomeric ssDNA, where telomere elongation by telomerase happens, TRF1-initiated POT1 loading to the telomere 3' end via shelterin interactions is believed to directly block telomerase from elongating telomeres (Loayza and De Lange, 2003). Shelterin architecture in fission yeast, *Schizosaccharomyces pombe*, closely resembles that of mammals (Miyoshi et al., 2008) (Figure 1A). Either its dsDNA binder Taz1 (homolog of hTRF1/2) (Cooper et al., 1997) or its ssDNA binder Pot1 (Baumann and Cech, 2001) can independently recruit other shelterin components, Rap1, Poz1 (hTIN2 homolog), and Ccq1, to telomeres (Miyoshi et al., 2008). Using *S. pombe* as a model system, we recently discovered that the complete linkage within the shelterin complex, rather than individual shelterin components per se, regulates the extendibility of telomeres by telomerase (Jun et al., 2013). Disruption of this linkage leads to unregulated telomere elongation. These previous studies emphasized a critical role of shelterin complex assembly in telomere length regulation. Indeed, several human POT1 variants were found to predispose to the development of familial melanoma and carriers of some of these mutations have elongated telomeres (Robles-Espinoza et al., 2014; Shi et al., 2014). These mutations may allow cancer cells to achieve replicative immortality, and thus provide the same outcome as previously identified TERT (telomerase reverse transcriptase) promoter mutations (Horn et al., 2013; Huang et al., 2013) that lead to cancer-specific TERT activation (Borah et al., 2015). Most of melanoma-associated POT1 mutations reside in the highly conserved oligonucleotide and oligosaccharide-binding (OB) domains of POT1, thereby disrupting POT1-telomeric ssDNA interaction (Robles-Espinoza et al., 2014; Shi et al., 2014). In addition, one mutation, Ala532Pro (A532P), was found in the C terminus of POT1, which contains the TPP1-binding domain (Shi et al., 2014). However, the mechanism by which POT1-A532P facilitates melanoma formation is still unknown. To understand the role of shelterin complex in regulating telomere states, we need to have accurate information about protein-protein interfaces between shelterin

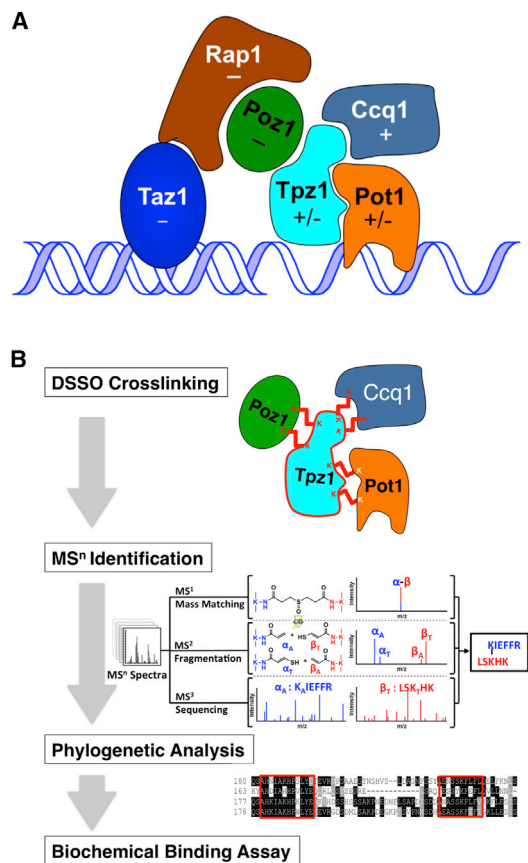


Figure 1. Fission Yeast Shelterin Complex and a Strategy—MICro-MS—to Dissect Its Interaction Interfaces

(A) Fission yeast shelterin complex is composed of telomeric sequence-specific double-stranded and single-stranded DNA binding proteins, Taz1 and Pot1, respectively, accompanied by their protein interaction partners, Rap1, Poz1, and Tpz1, forming a bridge between Taz1 and Pot1. If the deletion of a telomere protein causes telomere elongation, this protein is regarded as a negative regulator of telomere lengthening, and is therefore labeled “–”, otherwise, labeled “+”. For clarity, the stoichiometry of each individual component is not indicated in the figure and therefore only one copy of each component is shown.

(B) Schematic illustration of MICro-MS strategy to identify contact residues at the interfaces of protein interactions. The MS-cleavable crosslinker DSSO chemically crosslinks neighboring lysine (K) residue pairs of two interacting proteins, which, in turn, can be identified via sequencing protease-digested crosslinked peptide pairs by multistage tandem mass spectrometry. The identified crosslinked residues are then mapped to the phylogenetically compiled sequence alignment. Around the locations of the crosslinked residues, mutations are individually introduced to the conserved residues. In vitro GST pull-down and/or in vivo co-immunoprecipitation assays are subsequently performed to evaluate the degree that introduced mutations disrupt the targeted protein-protein interaction.

components, and therefore a complete dissection of the individual interactions. However, obtaining structural information regarding this complex by X-ray crystallography or nuclear magnetic resonance (NMR) has proved challenging. Alternative approaches are needed to enable us to acquire protein interfaces information without the requirement for high-resolution structures.

In recent years, crosslinking mass spectrometry (XL-MS) has become an increasingly valuable tool for studying protein-protein interactions and structural interrogation of protein complexes due to technological advancement in mass spectrometry (MS) instrumentation, new development of crosslinking reagents and bioinformatics tools to facilitate MS analysis of crosslinked peptides (Erzberger et al., 2014; Kaake et al., 2014; Kao et al., 2011, 2012; Politis et al., 2014; Walzthoeni et al., 2013; Yang et al., 2012), and an innovative algorithm developed for integrative structural biology utilizing distance restraints obtained from inter-subunit chemical crosslinking (Velázquez-Muriel et al., 2012). XL-MS studies involve protein crosslinking through a chemical linker simultaneously reacting with two amino acids that are in proximity to each other. Digestion of the crosslinked protein complex followed by peptide sequencing leads to the identification of crosslinked peptides, and consequently, proximal residue pairs. Because these crosslinked residues are constrained by the length of the linker used, the distribution of the crosslinked residue pairs helps probe protein-protein proximity. Unlike X-ray crystallography or NMR, XL-MS does not require samples with high concentration and purity. It also captures interactions from dynamic states, thus making it applicable to a broad range of protein complexes. However, XL-MS has proved challenging due to the complex fragmentation pattern of crosslinked peptides, which frequently prevents unambiguous identification of the crosslinked sequences. Recently, a new class of MS-cleavable crosslinker, disuccinimidyl sulfoxide (DSSO) was developed, which contains two symmetric MS-cleavable sites that preferentially cleave prior to the breakage of peptide backbones during collision-induced dissociation (CID) (Kao et al., 2011). In combination with multistage mass spectrometry (MSⁿ) and tailored bioinformatics tools, DSSO-based XL-MS workflow enables easy interpretation and unambiguous identification of crosslinked peptides and has proved effective in elucidating structures of protein complexes (Kao et al., 2011, 2012).

In this study, we have developed a strategy MICro-MS (*Mapping Interfaces via Crosslinking-Mass Spectrometry*) by combining DSSO-based XL-MS workflow, phylogenetic sequence analysis, and in vitro binding assays to identify protein-protein interaction interfaces without the need of obtaining high-resolution 3D structure of the complex. With this strategy, we comprehensively probed protein-protein proximity in Tpz1-centered complex in fission yeast shelterin and identified separation-of-function mutants of Ccq1, Poz1, or Pot1 that selectively disrupt their respective interactions with Tpz1. The identified mutants further reveal the critical regulatory roles of Tpz1 in telomere maintenance. We also found that POT1-A532P, a melanoma-associated POT1 mutation (Shi et al., 2014), lies in the POT1-TPP1 interface and causes weakened TPP1-POT1 interaction. Just as disrupting POT1-telomeric ssDNA interaction in other POT1 mutants predisposed to melanoma, such as Y89C, Q94E, R273L, and S270N (Robles-Espinoza et al., 2014; Shi et al., 2014), defective TPP1-POT1 interaction by hPOT1-A532P mutation equivalently breaks the complete shelterin linkage between telomeric dsDNA and ssDNA. Therefore, our work links shelterin connectivity to tumorigenesis. In addition, our MICro-MS strategy of identifying separation-of-function mutants to dissect protein complexes for

functional examinations will be generally applicable to other important multi-component protein complexes in the cell.

RESULTS

Identifying Contact Residues in Protein-Protein Interaction Interfaces by MICro-MS

We set out to utilize chemical crosslinking coupled with mass spectrometry (XL-MS) to identify contact residues located in the interfaces of interacting telomere shelterin components. Since mutations of the contact residues can selectively disrupt defined interactions within shelterin components, this strategy will allow us to identify separation-of-function mutants of shelterin components. Separation-of-function mutants can selectively block specific interactions without disrupting overall protein complex architecture. Thus, they should poise us to elucidate the roles of specific shelterin interactions in telomere maintenance without perturbing their roles in chromosome end protection.

The general workflow is depicted in [Figure 1B](#), in which DSSO crosslinking of purified protein complexes was first carried out to covalently connect residues within certain three-dimensional distance in the protein pairs that are specifically reactive to the crosslinker. Although the crosslinked residues in the protein complex might not be directly involved in mediating protein-protein interactions, they should at least be close to each other surrounding the interface. Therefore, the locations of the crosslinked residues point out where the binding interface is likely to be. The optimal crosslinking conditions were used to yield sufficient amounts of crosslinked products as evaluated by SDS-PAGE. The resulting crosslinked protein complexes were digested either in-solution or in-gel with trypsin and/or chymotrypsin to obtain the maximum coverage of detectable crosslinked peptides for LC-MSⁿ analysis. The mass to charge ratios of DSSO-crosslinked peptides were first measured during MS¹ analysis, and they were then subjected to collision induced dissociation (CID) during MS². Due to the presence of the robust sulfoxide C-S cleavage sites in the linker region, MS² analysis of a DSSO inter-linked peptide would lead to physical separation of the two crosslinked peptide constituents, thus allowing for MS³ sequencing of single peptide chains and subsequent identification using conventional database searching tools ([Kao et al., 2011](#)). Integration of the MSⁿ data (i.e., MS¹, MS², and MS³) results in simplified and unambiguous identification of DSSO-crosslinked peptides ([Kao et al., 2011](#)).

After identifying the crosslinked peptides and localizing lysine residues conjugated by DSSO, we mapped these residues to the phylogenetically compiled sequence alignment. We reasoned that functionally important residues (such as those for enzymatic activity, structural-fold determination, and protein complex assembly) should be evolutionarily conserved, and therefore represent leading candidates that contribute to protein-protein interactions. We introduced mutations to the conserved residues, especially the hydrophobic residues among them (as they constitute the hydrophobic core of protein-protein interactions), within approximately 8 to 15 amino acids from the crosslinked lysines, particularly in the regions where multiple lysine residues were identified as crosslinking points. In vitro GST

pull-down and in vivo co-immunoprecipitation assays were subsequently performed to evaluate the degree that the introduced mutations can disrupt the targeted protein-protein interaction. Mutations of the contact residues in the protein-protein interaction interface should efficiently disrupt the protein interaction. We termed this integrated strategy to identify separation-of-function mutants disrupting specific protein interaction interfaces *MICro-MS—Mapping Interfaces via Crosslinking-Mass Spectrometry*.

Benchmarking MICro-MS with 3D Structure of Proteasome Subunits Rpn8-Rpn11 Complex

Next, we assessed the applicability of MICro-MS to a protein complex with determined high-resolution 3D structure. In 2012, DSSO-based XL-MS strategy was employed to unravel the structural topology of *Saccharomyces cerevisiae* 19S proteasome regulatory particle ([Kao et al., 2012](#)). Five inter-subunit, DSSO-mediated crosslinks were identified between Rpn8 and Rpn11 subunits, suggesting their spatial proximity as well as potential direct protein interaction interfaces between Rpn8 and Rpn11. In 2014, two groups independently solved the crystal structure of heterodimer of the MPN (Mpr1–Pad1–N-terminal) domains of Rpn8 (1–179) and Rpn11 (2–239) ([Pathare et al., 2014](#); [Worden et al., 2014](#)). These two subunits primarily interact with each other through α helices forming two distinct interfaces. Interestingly, two pairs of DSSO-crosslinked lysines, Rpn8-K7:Rpn11-K218 and Rpn8-K28:Rpn11-K96, appear to be close to interface A and interface B, respectively, as shown in [Figures 2A–2C](#). The rest three identified lysine-crosslinks locate in the residues beyond the MPN domains and thus are not covered in the crystal structure. From the 3D structure, we calculated distances between the crosslinked lysine pairs to be 19.4 and 18.3 Å, respectively, falling in the range of DSSO effective reaction distance (~ 20 Å). In *Interface A* (shown in [Figure 2B](#)), the hydrophobic core of the interface is formed by four-helix bundle between $\alpha 1$, $\alpha 4$ of Rpn8 and $\alpha 1$, $\alpha 4$ of Rpn11. Specifically, side chains from residues L15, L16, and L19 in $\alpha 1$ of Rpn8 and residues M212, L216 and L213 in $\alpha 4$ of Rpn11 are the essential constituents of the hydrophobic interface. Remarkably, these interface residues are adjacent (within 15 amino acids) in primary sequence to the crosslinked lysines—K7 in Rpn8 and K218 in Rpn11, respectively. Moreover, they belong to the most phylogenetically conserved residues around the crosslinking sites ([Figures S1A and S1B](#)). *Interface B* (shown in [Figure 2C](#)) is located between $\alpha 2$ of Rpn8 and $\alpha 2$ of Rpn11. A cluster of four methionines: M76 and M79 from Rpn8 as well as M91 and M94 from Rpn11 build the core of the interface, which is flanked by salt bridges between Rpn8-R24 and Rpn11-T98 and between Rpn8-D20 and Rpn11-R100. Identified DSSO-crosslinked lysine pair Rpn8-K28:Rpn11-K96 lies at the edge of the interface, very close to the interface residues in primary sequence. Evidently, our benchmarking results demonstrate a strong correlation between DSSO-crosslinked lysine pairs and contact residues in protein-interaction interfaces in the primary sequence. Thus, we are set out to utilize MICro-MS to identify contact residues in interaction interfaces of protein complexes with no existing high-resolution 3D structure.

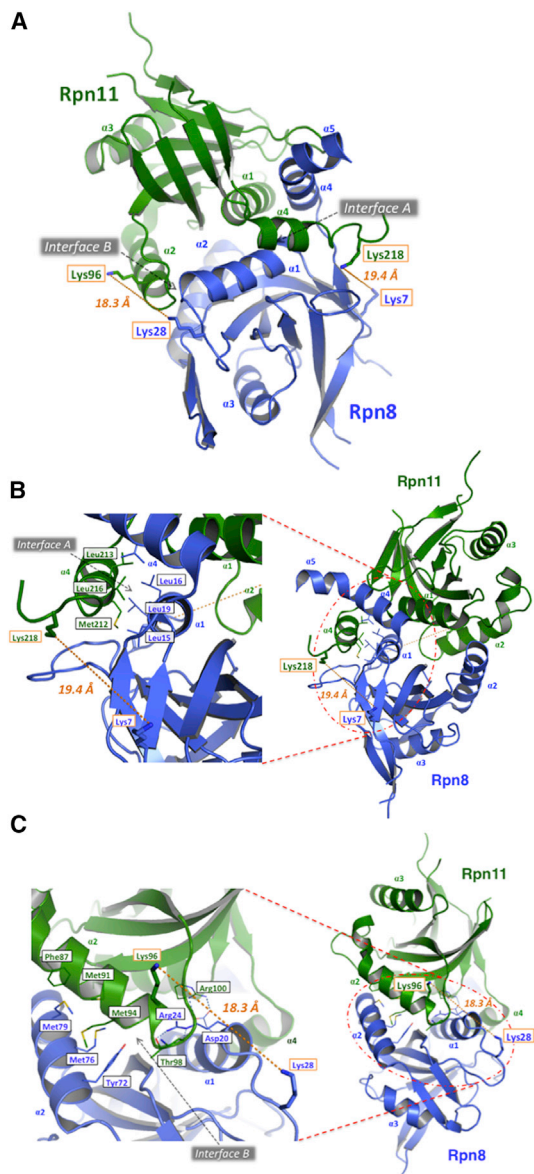


Figure 2. Benchmarking MICRo-MS Using Rpn8-Rpn11 Complex

(A) Crystal structure of Rpn8-Rpn11 heterodimer is presented with Rpn8 colored in blue and Rpn11 colored in green. The two interfaces are designated as Interface A and Interface B. The crosslinked lysines boxed in orange are connected with orange dashed lines; the distances between the lysine pairs are shown next to the lines.

(B) Close-up view showing a DSSO-crosslinked lysine pair (Rpn8-K7:Rpn11-K218) and interface A nearby in Rpn8-Rpn11 complex. The hydrophobic core of the interface is formed by four-helix bundle between α_1 , α_4 of Rpn8 and α_1 , α_4 of Rpn11. Specifically, side chains from residues L15, L16, and L19 (labeled in blue) in α_1 of Rpn8 and residues M212, L216, and L213 (labeled in green) in α_4 of Rpn11 are the essential constituents of the hydrophobic interface.

(C) Close-up view showing a DSSO-crosslinked lysine pair (Rpn8-K28:Rpn11-K96) and interface B nearby in Rpn8-Rpn11 complex. Interface B is located between α_2 of Rpn8 and α_2 of Rpn11. A cluster of four methionines: M76 and M79 from Rpn8 (labeled in blue) as well as M91 and M94 from Rpn11 build the core of the interface (labeled in green), which is flanked by salt bridges between Rpn8-R24 and Rpn11-T98 and between Rpn8-D20 and Rpn11-R100.

Dissecting the Ccq1-Tpz1 Interacting Interface via MICRo-MS

Tpz1, the fission yeast homolog of the mammalian shelterin component TPP1 (Houghtaling et al., 2004; Liu et al., 2004; Sexton et al., 2014; Wang et al., 2007; Ye et al., 2004), is a linchpin molecule interacting with three other shelterin components—Ccq1, Poz1 via its C-terminal domain (Tpz1-CTD), and with Pot1 using its N-terminal domain (Tpz1-NTD) (Figure 1A) (Miyoshi et al., 2008). Our previous work identified Tpz1 mutants that selectively disrupt the ability of Tpz1 to interact with each of its interacting partners and revealed an interesting interplay among the positive and negative regulators of telomere length homeostasis (Jun et al., 2013). To achieve a complete dissection of the protein-protein interactions between Tpz1 and its interacting shelterin components, and therefore to define the boundary between positive and negative telomere regulators, we decided to further map the Tpz1-interacting surfaces on Ccq1, Poz1, and Pot1, respectively.

Ccq1 is more than 700 amino acids long, and it is extremely labor intensive and tedious to identify its point mutations that disrupt Ccq1-Tpz1 interaction via mutating every phylogenetically conserved residue in Ccq1. We set out to gather interface information by utilizing MICRo-MS strategy. As Ccq1 (130–439) interacts with Tpz1 (415–458), we co-expressed recombinant Ccq1 (130–439) with Tpz1 (415–458) in *E. coli* and purified the complex. We then subjected the complex to chemical crosslinking using an optimized concentration of DSSO—5.0 mM. As shown in Figure 3A, the crosslinked Ccq1 (130–439) and Tpz1 (415–458) complex was observed, while the free form of both Ccq1 (130–439) and Tpz1 (415–458) decreased concomitantly. The covalently crosslinked Ccq1 (130–439)/Tpz1 (415–458) shows molecular weight of ~72 kDa. This agrees with the Ccq1-Tpz1 complex forming a dimer of Ccq1-Tpz1 heterodimer, as we observed in gel filtration analysis, in which the protein complex was examined in its native form (Figure S2A). The tryptic digests of crosslinked Ccq1-Tpz1 complexes were then analyzed by LC-MSⁿ. Figure 3B illustrates a representative MSⁿ analysis for unambiguous identification of DSSO crosslinked peptides. As shown, MS² analysis of a selected peptide (m/z 554.0333⁴⁺) yielded two peptide fragment pairs, i.e., α_A/β_T (m/z 420.75²⁺/678.31²⁺) and α_T/β_A (m/z 432.20²⁺/662.83²⁺), which is characteristic to a hetero-inter-linked peptide (α - β) (Kao et al., 2011). Each fragment (α_A , β_T , α_T , or β_A) represents one of the two crosslinked peptide constituents modified with the defined remnants of the linker after its cleavage, thus suggesting this peptide is a DSSO inter-linked peptide. The dominant fragment pair ions (α_A/β_T) were subsequently subjected to MS³ analysis, in which the series of b ($b_2\sim b_5$) and y ($y_1\sim y_5$) ions detected for the α_A fragment unambiguously identified it as ¹⁷¹IQEKA_{IR}¹⁷⁶ of Ccq1, while the series of b ($b_2\sim b_7$, b_9) and y ($y_2\sim y_3$, y_5 , $y_7\sim y_9$) ions detected for β_T unambiguously identified the peptide as ⁴³⁴K_TPIPDYDFM(Ox)K⁴⁴³ of Tpz1. Finally, integration of the MSⁿ data precisely identifies the inter-link between

Identified DSSO-crosslinked lysine pair Rpn8-K28:Rpn11-K96 (linked by an orange dash line) lies at the edge of the interface, very close to the interface residues in primary sequence.

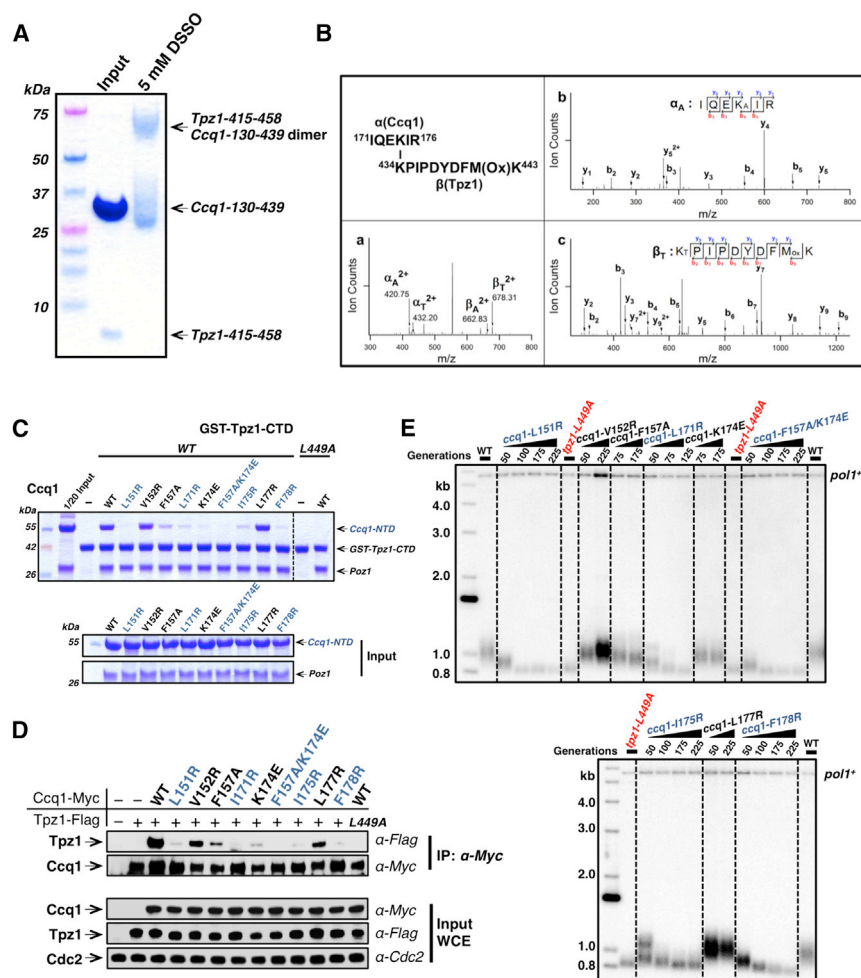


Figure 3. Dissecting Ccq1-Tpz1 Interacting Interface via MICro-MS

(A) SDS-PAGE of Ccq1 (130–439) and Tpz1 (415–458) complex before and after being crosslinked by DSSO.

(B) (a) MS² spectrum of a quadruply charged crosslinked peptide α - β (m/z 554.2863⁴⁺), in which two characteristic peptide fragment pairs were detected: α_A/β_T (m/z 420.75²⁺/678.31²⁺) and α_T/β_A (m/z 432.20²⁺/662.83²⁺). MS³ spectra of (b) α_A (m/z 420.75²⁺) and (c) β_T (m/z 678.31²⁺) fragment ions detected in (a), which unambiguously identified their sequences as IQEK_AIR of Ccq1 and K_TPIPDYDFM_{Ox}K of Tpz1, respectively, demonstrating a linkage between residue K174 of Ccq1 and K434 of Tpz1. K_A, alkene-modified lysine; K_T, unsaturated thiol-modified lysine.

(C) In vitro GST pull-down assays testing the binding of Ccq1 mutants and Poz1 to GST-Tpz1-CTD (406–508). GST-Tpz1-CTD-L449A serves as the negative control. Input: 1/20 of Ccq1 and 1/5 Poz1 before their incubation with GST-Tpz1-CTD.

(D) Co-immunoprecipitation (coIP) assays evaluating the binding between full-length Tpz1 and Ccq1 mutants. *tpz1-L449A* serves as the negative control. Cdc2 was shown as the loading control. Input: 1/30 of input WCE (whole-cell extract).

(E) Southern blot analysis of EcoRI-digested genomic DNA using the telomere DNA probe for the indicated *ccq1* mutant strains from successive re-streaks on agar plates. *ccq1* mutants disrupting Ccq1-Tpz1 interaction have shorter telomeres. In the telomere length analysis southern blots presented in this paper, the 1 kb plus marker from Life Technologies is used. Wild-type cells are denoted as “WT” in the blot. *pol1+* indicates the EcoRI-digested *pol1+* DNA fragment as loading control.

Tpz1-K434 and Ccq1-K174, suggesting their close proximity in three-dimensional space. Based on our previous study, Tpz1-L449A is able to disrupt Ccq1-Tpz1 interaction both in vitro and in fission yeast cells. The MSⁿ identification of Tpz1-K434 and Ccq1-K174 crosslinked by DSSO in the Tpz1-Ccq1 complex (Figure 3B) is remarkable, because Tpz1-K434 is only 15 amino acids away from the previously confirmed Ccq1-interacting site on Tpz1 (L449) (Jun et al., 2013). We therefore suspected that Ccq1 residues that mediate Ccq1-Tpz1 interaction should also be around K174 of Ccq1, the residue crosslinked to Tpz1-K434. Next, we introduced point mutations individually to several conserved residues around the K174 region of Ccq1 (Figure S2B), and then the purified recombinant Ccq1 mutants produced in *E. coli* were subjected to GST pull-down assays to evaluate their binding ability to GST-Tpz1-CTD. As shown in Figure 3C, among nine Ccq1 mutants, Ccq1-L151R and Ccq1-F157A/K174E completely abolished association between Ccq1 and Tpz1. In addition, Ccq1-L171R, Ccq1-K174E, Ccq1-I175R, and Ccq1-F178R all significantly diminished Ccq1-Tpz1 interaction, whereas Ccq1-V152R and Ccq1-L177R still retain wild-type binding to Tpz1. Furthermore, we also confirmed that Ccq1 mutations, which interfere with

Ccq1-Tpz1 interaction in vitro, also affect full-length Ccq1-Tpz1 interaction to the similar degree in co-immunoprecipitation assays (Figure 3D); however, they still maintain their interactions with Clr3—the interaction partner of Ccq1 in the SHREC complex (Sugiyama et al., 2007) (Figure S2C). In addition, chromatin immunoprecipitation (ChIP) analysis of these Ccq1 mutants indicates that they can localize to telomeres as well (Figure S2D). Therefore, we identified separation-of-function mutants of Ccq1, specifically disrupting Ccq1-Tpz1 interaction.

After obtaining Ccq1 mutants disrupting Ccq1-Tpz1 interaction, we further asked whether these Ccq1 mutants eliminate the function of Ccq1 as a positive regulator of telomere length. As predicted, telomere length in *ccq1-L151R* and *ccq1-F157A/K174E pombe* cells, in which Ccq1-Tpz1 interaction is completely abolished, is stable but ~150 bp shorter than that in the wild-type cells, reminiscent of *tpz1-L449A* cells (Figures S2E and 3E) (Armstrong et al., 2014; Jun et al., 2013). *S. pombe* cells bearing *ccq1+* mutations that significantly diminish Ccq1-Tpz1 interaction, such as *ccq1-L171R*, *ccq1-I175R*, and *ccq1-F178R*, also have similarly shorter telomeres as *tpz1-L449A* cells. However, cells bearing *ccq1+* mutations, *ccq1-V152R* and *ccq1-L177R*, which have little effect on

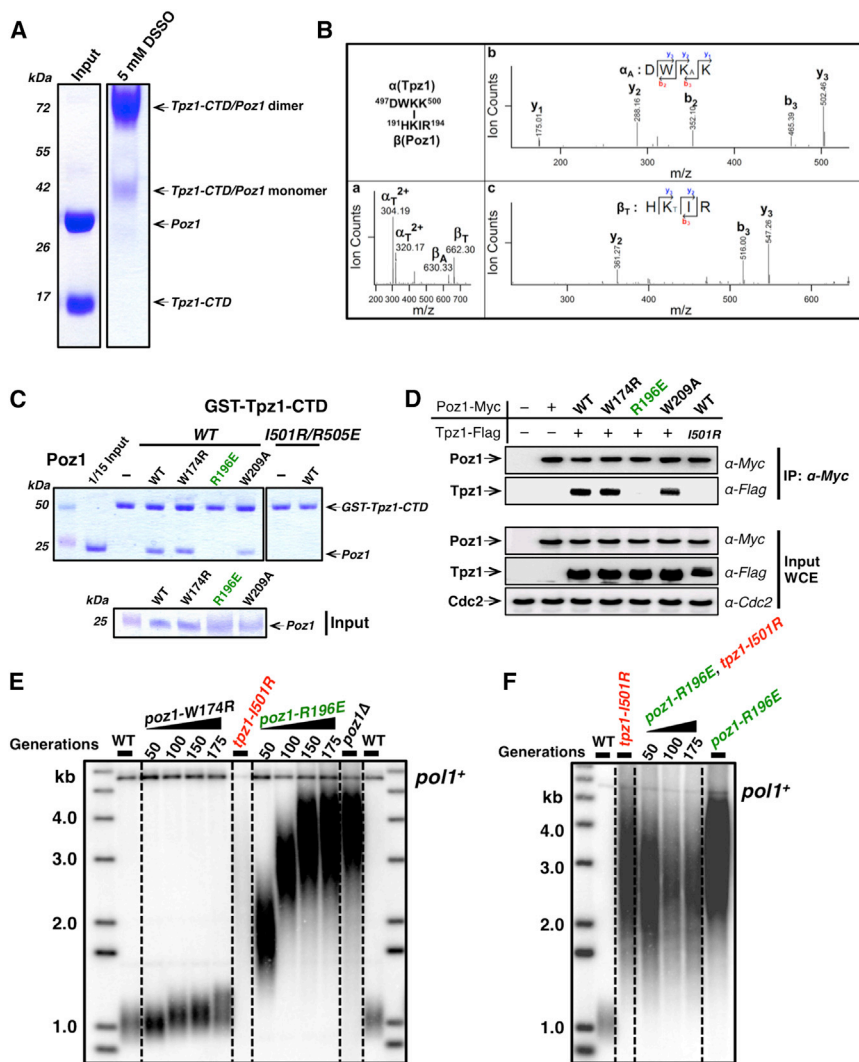


Figure 4. A Poz1 Mutation that Prevents Tpz1 Binding Results in Dramatic Telomere Elongation

(A) SDS-PAGE of full-length Poz1 and Tpz1 (406–508) complex before and after being crosslinked by DSSO.

(B) (a) MS² spectrum of a triply charged cross-linked peptide α - β (m/z 429.5608³⁺) in which two characteristic peptide fragment pairs were detected: α_A/β_T (m/z 304.19²⁺/662.30⁺) and α_T/β_A (m/z 320.17²⁺/630.33⁺). MS³ spectra of (b) α_A (m/z 304.19²⁺) and (c) β_T (m/z 662.30⁺) fragment ions detected in (a), which unambiguously identified their sequences as DWK_AK of Tpz1 and HK_TIR of Poz1, respectively, demonstrating a linkage between residue K192 of Poz1 and K499 of Tpz1. K_A, alkene-modified lysine; K_T, unsaturated thiol-modified lysine.

(C) In vitro GST pull-down assays testing the binding of Poz1 mutants to GST-Tpz1-CTD (406–508). Poz1-R196E (colored in green) is defective in binding to GST-Tpz1-CTD. GST-Tpz1-CTD-I501R/R505E serves as the negative control. Input: 1/15 of the samples before their incubation with GST-Tpz1-CTD.

(D) *poz1-R196E* disrupts Poz1-Tpz1 interaction as evaluated by coIP assays. *tpz1-I501R* serves as the negative control. Cdc2 was shown as the loading control. Input: 1/30 of input WCE.

(E) Telomere length analysis southern blots for the indicated *poz1* mutant strains from successive restreaks on agar plates. *poz1-R196E* causes telomere elongation.

(F) Double-mutant strain *poz1-R196E/tpz1-I501R* cells have elongated telomeres similar to those of *poz1-R196E* or *tpz1-I501R* cells.

Ccq1-Tpz1 interaction, maintain wild-type telomere length. Furthermore, *tpz1-L449A/ccq1-F157A/K174E* double-mutant cells have an almost identical telomere phenotype as either *ccq1-F157A/K174E* or *tpz1-L449A* cells (Figure S2F), indicating the mutations, either in Tpz1 or in Ccq1, affect the same functionality in telomere maintenance pathway. Much like *tpz1-L449A* cells, which maintain their short telomeres via homologous recombination pathway involving *rad51*⁺, *ccq1-F157A/K174E* cells also require *rad51*⁺ to maintain their telomeres as deletion of *rad51*⁺ in *ccq1-F157A/K174E* immediately abrogates the stably maintained short telomeres in *ccq1-F157A/K174E* cells (Figure S2G). Taken together, utilizing MICro-MS, we were able to identify Ccq1 mutants that are defective in interacting with Tpz1, and we found that these Ccq1 mutants are functionally equivalent to *tpz1-L449A* in telomere maintenance.

A Poz1 Mutation that Prevents Tpz1 Binding Results in Dramatic Telomere Elongation

Having successfully employed MICro-MS to dissect Ccq1-Tpz1 interaction, we next applied this approach to define the signifi-

cance of the Poz1-Tpz1 interaction. Using the same procedure as described above for Ccq1-Tpz1 complex, we analyzed DSSO-crosslinked Poz1-Tpz1 complex (Figure 4A) to identify crosslinked peptides and the lysine pairs that make the linkages. Interestingly, Tpz1-K499, a residue adjacent to Tpz1-I501—a previously identified Poz1-interacting residue in Tpz1 (Jun et al., 2013), was found to crosslink to K180, K190, and K192 of Poz1 (Figures 4B, S3A, and S3B). In addition, Tpz1-K500 was also observed to crosslink to Poz1-K190 (Figure S3C). This result suggests that a region around K180 and K192 of Poz1 may contain Tpz1 contact sites (Figure S3D). We therefore introduced mutations individually to three conserved residues around this region, Poz1-W174R, R196E, and W209A, and performed GST pull-down assay to evaluate their Tpz1 binding ability. Among these three Poz1 mutants, only Poz1-R196E completely abrogated Poz1-Tpz1 interaction as shown in Figure 4C. Accordingly, we found that Poz1-R196E also caused loss of Poz1-Tpz1 interaction in the *S. pombe* cells as detected by co-immunoprecipitation assays (Figure 4D).

We generated a yeast strain carrying the *poz1-R196E* mutation to evaluate its importance for telomere length homeostasis. *poz1-R196E* mutant cells had dramatically elongated telomeres (Figures 4E and S3E), consistent with the phenotype previously

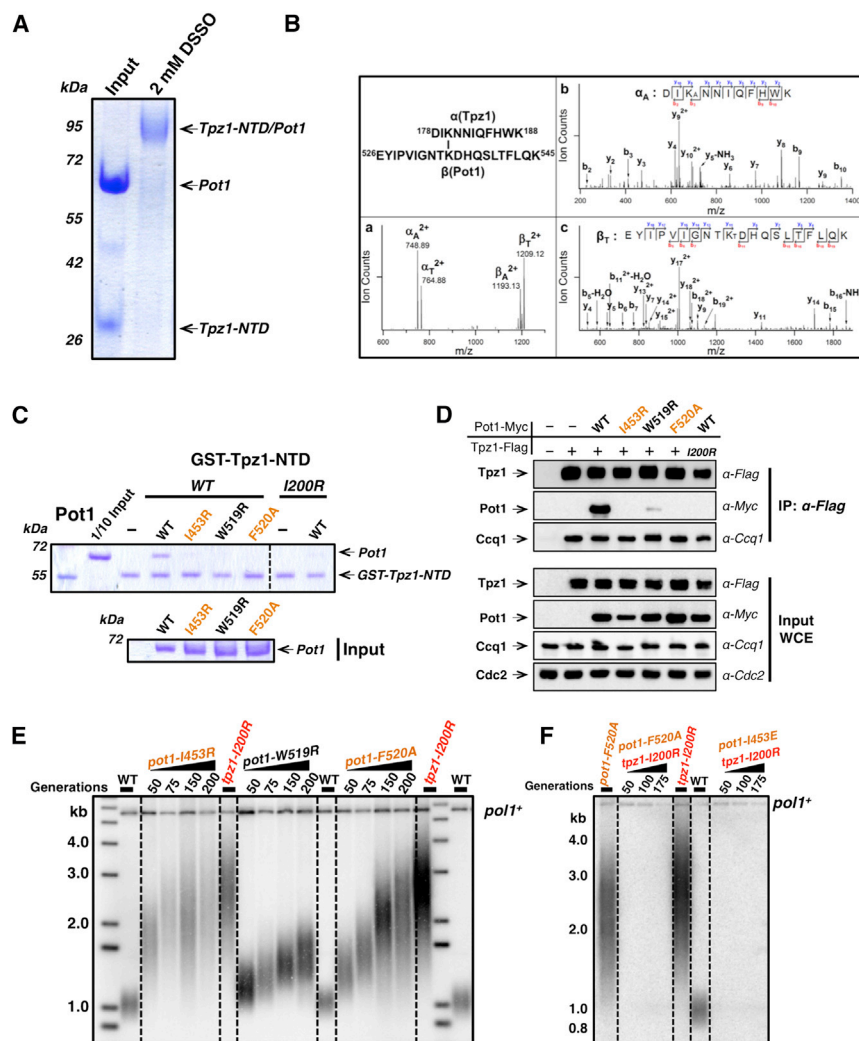


Figure 5. Pot1 Is a Negative Regulator of Telomere Length and Protects Telomeres Redundantly with Tpz1

(A) SDS-PAGE of full-length Pot1 and Tpz1-NTD (1–234) complex before and after being cross-linked by DSSO.

(B) (a) MS² spectrum of a quadruply charged crosslinked peptide α - β (m/z 983.5108⁴⁺) in which two characteristic peptide fragment pairs were detected: α_A/β_T (m/z 749.89²⁺/1209.12²⁺) and α_T/β_A (m/z 764.88²⁺/1193.13²⁺). MS² spectra of (b) α_A (m/z 748.89²⁺) and (c) β_T (m/z 1209.12²⁺) fragment ions detected in (a), which unambiguously identified their sequences as DIK_AANNIQFHWK of Tpz1 and EYIPVIGNTK_TTDHQSLTFLQK of Pot1, respectively, indicating a linkage between residue K180 of Tpz1 and K535 of Pot1. K_A, alkene-modified lysine; K_T, unsaturated thiol-modified lysine.

(C) In vitro GST pull-down assays testing the binding of Pot1 mutants to GST-Tpz1-NTD (2–234). Pot1-1453R and Pot1-F520A (colored in orange) abolish the in vitro interaction with GST-Tpz1-NTD. GST-Tpz1-NTD-I200R serves as the negative control. Input: 1/15 of the samples before their incubation with GST-Tpz1-NTD.

(D) CoIP assays evaluating the binding of Pot1 mutants and Ccq1 to full-length Tpz1. *pot1-1453R* and *pot1-F520A* completely disrupt Pot1-Tpz1 interaction. *tpz1-I200R* serves as the negative control. Cdc2 was shown as the loading control. Input: 1/30 of input WCE.

(E) Telomere length analysis southern blots for the indicated *pot1* mutant strains for successive re-streaks on agar plates. *pot1-1453R* and *pot1-F520A* strains, in which Pot1-Tpz1 interaction is disrupted, have elongated telomeres.

(F) Telomere deprotection phenotype was observed in both *pot1-F520A/tpz1-I200R* and *pot1-1453R/tpz1-I200R* double mutants.

observed for *tpz1-I501R* mutant strain (Jun et al., 2013), which also fails to form the Poz1-Tpz1 complex. Moreover, when *poz1-R196E* was coupled with *tpz1-I501R*, the double mutant also showed elongated telomere, similar to *poz1-R196E* single mutant with no additional telomere elongation (Figure 4F). These results indicate that Poz1-R196 is indeed functionally equivalent to Tpz1-I501 in mediating Tpz1-Poz1 interaction, a key linkage point in the negative regulation force imposed by shelterin complex upon telomerase.

Pot1 Is a Negative Regulator of Telomere Length and Protects Telomeres Redundantly with Tpz1

In *S. pombe*, Pot1 is the direct single-stranded telomeric DNA binder and is responsible for telomere 3' end protection by forming a complex with Tpz1 (Miyoshi et al., 2008). Deletion of either protein can result in chromosome circularization, whereas disruption of Tpz1-Pot1 interaction by the Tpz1-I200R mutation conversely leads to telomere elongation (Jun et al., 2013). Pot1 interacts with the N-terminal domain of Tpz1 (Tpz1-NTD), which is distinct from Ccq1 and Poz1 binding regions in the C-terminal

domain of Tpz1 (Tpz1-CTD). To achieve the complete dissection of the interfaces in Tpz1-mediated negative regulation of telomere elongation, we aimed to identify regions in Pot1 that mediate its interaction with Tpz1-NTD. As shown in Figure 5A, efficient crosslinking by DSSO was achieved with the purified Pot1-Tpz1-NTD complex. Further MSⁿ analyses revealed that two lysine residues (K180 and K226) in proximity to I200 position of Tpz1 were crosslinked to Pot1 (K403, K535, and K553) (Figures 5B and S4A–S4C). To design separation-of-function mutations in Pot1 for specific disruption of the Pot1-Tpz1 interaction, several conserved residues around the crosslinked lysines were mutated (Figure S4D), and the mutants were tested for their interactions with Tpz1 both in vitro (by GST pull-down) (Figure 5C) and in vivo (by co-immunoprecipitation) (Figure 5D). We found that Pot1-1453R and Pot1-F520A completely disrupt Pot1-Tpz1 binding both in vitro and in vivo. In addition, we examined the crystal structure of the *Oxytricha nova* homolog of Pot1-Tpz1 complex—TEBP- α/β (Horvath et al., 1998) and found that secondary structure prediction of Pot1 imposed onto its homologous TEBP- α/β structure placed I453 and F520 of Pot1 at the

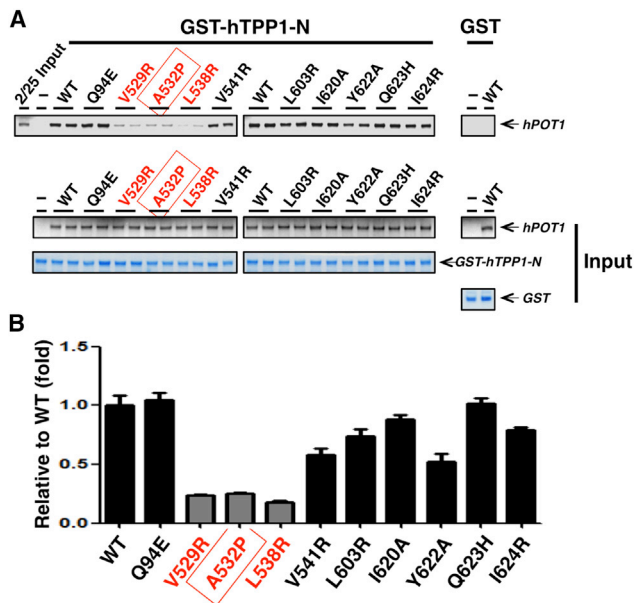


Figure 6. A Human Family Melanoma-Associated POT1 Variant Has Compromised hPOT1-hTPP1 Interaction

(A) In vitro GST pull-down assays testing the binding of hPOT1 mutants to GST-hTPP1-NTD (89–334). hPOT1-A532P (boxed in red) was identified in familial melanoma patients. hPOT1-V529R and hPOT1-L538R (boxed in red) also negatively affect the interaction between hPOT1 and GST-hTPP1-NTD. All hPOT1 (WT and mutants) are labeled with ^{35}S and visualized by Bio-Rad Phosphorimager. GST-hTPP1-NTD and GST are visualized by Coomassie blue staining.

(B) Quantification of the binding between GST-hTPP1-NTD and hPOT1 mutants from (A). The interaction between GST-hTPP1-NTD and hPOT1-WT is set to 1.

protein interaction interface (Figure S4D), consistent with our binding data. We performed ChIP analyses to evaluate telomeric localizations of Pot1 and Ccq1 in Pot1-Tpz1 interaction-defective Pot1 mutant strains (Figures S4E and S4F), demonstrating that these mutations only disrupt Pot1-Tpz1 interaction with minimum effect on Pot1 or Ccq1 telomere association. In agreement with this, we found that these Pot1 mutants can bind to telomeric ssDNA in gel-shift assays (Figure S4G). Reminiscent of *tpz1-1200R* cells, telomeres in both *pot1-I453R* and *pot1-F520A* mutant cells are elongated (Figures 5E and S4H) (Jun et al., 2013), indicating that Pot1 is also a negative regulator of telomere length. However, when we coupled *pot1-I453R* or *pot1-F520A* with *tpz1-1200R*, the double mutant showed no telomere signal, with part of the subtelomeric regions disappeared concomitantly (Figures 5F and S4I). These results strongly suggest that there is an alternative pathway that Tpz1 is involved in, in addition to the Pot1 pathway, to redundantly protect telomere erosion.

In summary, we have successfully employed MICRo-MS to comprehensively map Tpz1-centered protein-protein interfaces in fission yeast shelterin. As a result, we successfully identified mutants of Ccq1, Poz1, and Pot1 that selectively disrupt their respective interactions with Tpz1, the linchpin molecule that is functionally positioned between the positive and negative regulators of telomere elongation.

A Human POT1 Variant in Family Melanoma Patients Has Compromised hPOT1-hTPP1 Interaction

Replicative telomere attrition is one of the key restriction mechanisms that form a key barrier to infinite cell proliferation. As a result, a hallmark of cancer cells is their ability to circumvent multiple regulatory mechanisms that normally restrict cell proliferation (Hanahan and Weinberg, 2011). The integrity of telomere shelterin structure is essential for telomere length homeostasis, which, in turn, enables the anti-proliferative barrier set by short telomeres (Günes and Rudolph, 2013). Indeed, it has been shown that long telomeres can bypass the requirement of telomerase activation in the process of tumorigenesis (Taboski et al., 2012). Recently, two studies have linked 4%–6% of familial melanoma cases to germline variants in the gene encoding human POT1, the first shelterin component found to be mutated in cancer (Robles-Espinoza et al., 2014; Shi et al., 2014). Among these hPOT1 variants, many alter key residues in the N-terminal OB domains of POT1, causing the inability of hPOT1 to bind to telomeric ssDNA and leading to longer telomeres (Robles-Espinoza et al., 2014; Shi et al., 2014). However, one familial melanoma hPOT1 variant (hPOT1-A532P) contains a point mutation in the C terminus of hPOT1, and therefore is unlikely to disrupt POT1-ssDNA binding. Given our knowledge gained from fission yeast Pot1-I453R, which disrupts Pot1-Tpz1 interaction and aligns to where hPot1-A532 locates (Figure S5), we suspected that the hPOT1-A532P mutation might reside in the TPP1 (human counterpart of fission yeast Tpz1) interaction surface. Thus, hPOT1-A532P might disrupt hPOT1-hTPP1 interaction, thereby facilitating tumorigenesis by causing inappropriate telomere elongation, similar to fission yeast Pot1-I453R. To test this possibility, we in vitro translated hPOT1 and its mutants and evaluated their binding abilities to GST-hTPP1-NTD. Notably, hPOT1-A532P, as well as two other mutants in the adjacent regions, hPOT1-V529R and L538R, has significantly weakened hPOT1-hTPP1 interaction (Figures 6A and 6B). This result emphasizes the importance of the intact “shelterin bridge” in telomere length regulation and explains how mutations in a shelterin component overcome the replicative telomere barrier, and thus lead to tumorigenesis.

DISCUSSION

MICRo-MS Is Effective in Identifying Functional Protein-Protein Contact Residues

Identifying interfaces between protein components, and generating separation-of-function mutants thereafter, is a prerequisite for elucidating the functional role of each component in the large multi-protein complex, such as the shelterin complex at the end of our chromosomes. For proteins that have multiple interaction partners, such as Tpz1 in fission yeast shelterin complex, its separation-of-function mutants are absolutely required to elucidate the specific roles of each of these protein interactions. However, X-ray crystallography and NMR spectroscopy have been the main experimental techniques that provide the structural details of protein-protein interfaces, and consequently, the knowledge to design separation-of-function mutants. Both approaches are very time consuming, labor intensive, and extremely demanding on the chemical and biophysical behavior

of the protein complex. Thus, only a limited number of protein complexes are suitable for these high-resolution techniques. Here, utilizing XL-MS with a recently developed MS-cleavable linker DSSO, coupled with phylogenetic and biochemical analyses, we present an integrated strategy (Figure 1B) that successfully identified contact residues in Tpz1-centered protein-protein interfaces of fission yeast shelterin. The DSSO-based XL-MS workflow greatly facilitates the identification of cross-linked peptides, which, in turn, provides essential information about regions that are very likely to mediate protein-protein interactions. Phylogenetic analysis further narrows down the candidate residues to be mutated in the regions close to crosslinked residues, and, thereafter, GST pull-down assays identify residues directly involved in and contribute to the protein-protein interaction. This strategy can be directly applied to other protein complexes due to its simplicity, sensitivity, efficiency, accuracy, and speed. In addition, recent studies suggested the existence of evolutionarily co-varied residues as good candidates for contact residues across protein interaction interface because compensatory mutations occur in the interfaces to maintain interaction stability during evolution (Marks et al., 2011; Ovchinnikov et al., 2014; Weigt et al., 2009). Therefore, evolutionary covariation analysis can be combined with MICro-MS to more accurately identify interface residues by prioritizing candidate residues to mutate.

For MICro-MS, chemical crosslinking sets up the foundation for the overall outcome of this strategy. The linker length of the chemical crosslinker is crucial for linking residues pairs around the protein-interaction interface. DSSO has a linker length of 10.1 Å, resulting in potential linkages between lysines within ~20 Å. This is a distance that has been determined to be optimal for specifically crosslinking lysines across interfaces. When lysines are scarce in one of the interacting proteins or both, other crosslinking reagents targeting other amino acid residues such as cysteines or acidic residues (Leitner et al., 2014) can be utilized similarly to determine protein interaction contacts. Interfaces that are small can be potentially probed by crosslinkers with shorter linker length such as EDC (1-ethyl-3-(3-dimethylaminopropyl)carbodiimide hydrochloride), which targets acidic residues (D and E), with zero linker length. Incorporating CID-inducible cleavage group into chemical crosslinkers with different linker lengths and/or reactive groups targeting various side chains apparently has urgent need.

For structurally heterogeneous samples, crosslinking mass spectrometry has the advantage of probing proximal regions of interacting proteins in different conformations. Unlike most other biophysical techniques, in which sample heterogeneity interferes with the generation of characteristic signals, for MICro-MS, different protein interactions existing in different conformations can be identified as distinct crosslinking pairs with crosslinked peptide counts proportional to its population in the sample. Moreover, capturing stable interactions in general is much easier than identifying transient ones, but stability is not a requirement; this is another aspect of MICro-MS that allows the stabilization of transient complexes through chemical crosslinking for subsequent analysis to identify residues close to the interfaces. Finally, methods such as yeast two-hybrid and peptide arrays are known to identify binary interactions and have been used extensively to

identify domains that mediate protein interaction. They can also be utilized to identifying protein-protein interacting surfaces residues when coupled with alanine scanning of the whole or selected region of the protein pairs. In addition, once protein domains responsible for interaction are identified via yeast two hybrid, they can be subject to MICro-MS, which provides leading candidate residues for both methods to test, significantly reducing the number of residues to mutate. It is worth mentioning that MICro-MS allows the study of each individual interface in multi-protein complexes concurrently.

Shelterin Connectivity, Telomere Length Regulation, and Familial Melanoma

Our recent study of fission yeast shelterin revealed that the complete linkage within shelterin, connecting double-stranded and single-stranded telomeric DNA, governs the telomerase-nonextendible state of the telomere (Jun et al., 2013). In this study, taking advantage of XL-MS with a MS-cleavable linker strategy, we achieved complete dissection of Tpz1-centered shelterin component interactions (Tpz1-Ccq1, Tpz1-Poz1, Tpz1-Pot1) and obtained separation-of-function mutants that facilitate the investigation of their roles in telomerase regulation, telomere protection, and potentially other cellular functions such as telomere silencing (Tadeo et al., 2013) and meiosis. These mutants emphasize the importance of shelterin connectivity in negatively regulating telomerase as we concluded from Tpz1 separation-of-function mutants. This is because any mutation that disrupts the shelterin connectivity from dsDNA to ssDNA, no matter in Tpz1 or in the Tpz1 interacting partners, uniformly leads to over-elongated telomeres. They also make exploring the regulation of telomere length homeostasis by shelterin components, especially its activator Ccq1 (Webb and Zakian, 2012), possible.

In addition, our study also has clinical significance. Since fission yeast and human have homologous shelterin components and architecture, the shelterin interaction interface information obtained from fission yeast can be easily applied to the human shelterin. This information will not only help design separation-of-function mutants of human shelterin components, it will also offer mechanistic insights to a constellation of genetic diseases caused by impaired telomere maintenance due to defects in telomere shelterin. Human POT1 is the first member of shelterin components whose loss-of-function variants were found to predispose to human cancers, such as familial melanoma (Robles-Espinoza et al., 2014; Shi et al., 2014) and chronic lymphocytic (Ramsay et al., 2013; Speedy et al., 2014). Many identified POT1 mutations occurs in the N-terminal OB-fold domain that directly binds to the telomeric ssDNA. All four well-studied OB-fold domain mutants of hPOT1 identified in familial melanoma patients, e.g., POT1-Y89C, POT1-Q94E, POT1-R273L, and POT1-S270N, fail to bind to telomeric ssDNA and cause cells to have elongated telomeres (Robles-Espinoza et al., 2014; Shi et al., 2014). This can be mechanistically explained by the loss of complete linkage connecting telomeric dsDNA to ssDNA via shelterin, due to the inability of the mutants to bind to ssDNA, and thereby keeping the telomere constitutively in the extendible state. With sufficiently long telomeres reserve, tumorigenesis will not be impeded by the lack of telomerase in the cell, and cancer cells thus can automatically overcome the anti-proliferative

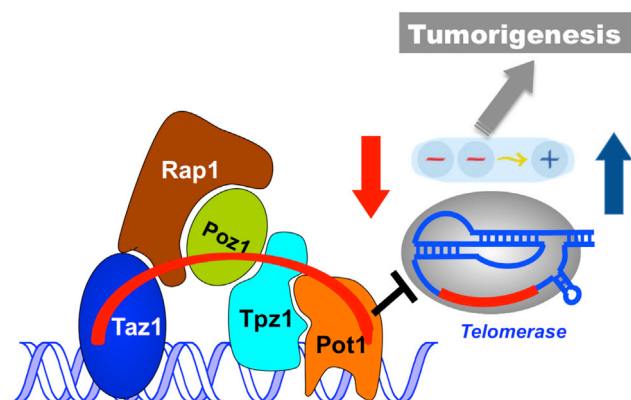


Figure 7. Model of Telomere Length Dysregulation-Related Tumorigenesis

Upregulation of positive regulators of telomere elongation (such as hTERT) is equivalent to downregulation of the negative regulators (such as the shelterin bridge) in leading to the deregulated telomere over-elongation, both helping the cancer cells to achieve replicative immortality, a key barrier to tumorigenesis.

barrier set by short telomeres (Taboski et al., 2012). Long telomeres help cells gain replicative time in order to accumulate other mutations (loss of function for tumor suppressor and gain of function for tumor activator). Exploiting homology between fission yeast and human shelterins, we find that another POT1 mutation (POT1-A532P), found in familial melanoma patients, affects POT1-TPP1 interaction. Based on what we learned from fission yeast, disrupting any point in the proteinaceous shelterin bridge between telomeric dsDNA and ssDNA would lead to elongated telomeres. Therefore, in that sense, defect in POT1-TPP1 interaction is equivalent to that in POT1-ssDNA interaction, both acting to downregulate the negative force of telomere elongation. Recently, in addition to POT1, point mutations clustered in the POT1-interacting domain of TPP1 were found in melanoma patients (Aoude et al., 2015), presumably disrupting POT1-TPP1 interaction just as POT1-A532P does. Interestingly, gain-of-function mutations in the hTERT promoter, which increase gene expression of hTERT, were recently found to be driver alterations in melanoma and other cancers (Horn et al., 2013; Huang et al., 2013). Upregulation of positive regulators of telomere elongation (such as hTERT) is equivalent to downregulation of the negative regulators (such as the shelterin bridge) (as shown in Figure 7) in leading to the deregulated telomere over-elongation, both helping the cancer cells to achieve replicative immortality, during and after the transformation.

EXPERIMENTAL PROCEDURES

Yeast Strains, Gene Tagging, and Mutagenesis

Fission yeast strains used in this study are listed in Table S1. Single mutant strains were constructed by one-step gene replacement of the entire open reading frame (ORF) with the selectable marker. Double- and triple-mutant strains were produced by mating, sporulation, dissection, and selection followed by PCR verification of genotypes. Genes were fused to specific epitope tags at the C terminus by homologous recombination; the pFA6a plasmid modules were used as templates for PCR (Bähler et al., 1998; Sato et al.,

2005). Point mutations were made by site-directed mutagenesis PCR using the high-fidelity polymerase *Pfu* (Agilent). All mutations were confirmed by DNA sequencing (Eton).

Protein Expression and Purification

Plasmids for recombinant protein expression in *E. coli* were transformed into Rosetta-BL21 (DE3) cells. Protein expression was induced with 0.4 mM isopropyl- β -D-1-thiogalactopyranoside (IPTG) for 4 hr at 30°C or 0.2 mM IPTG overnight at 16°C. Cells were disrupted by sonication in lysis buffer (25 mM Tris-HCl [pH 8.0], 350 mM NaCl, 15 mM imidazole, 5 mM β -mercaptoethanol, 1 mM PMSF, 2 mM benzamidine). The supernatant was incubated with Ni-NTA (QIAGEN) resin for 1 hr. After washing, the bound protein was eluted from the beads with elution buffer containing 300 mM imidazole. Some proteins were further purified with additional ion-exchange and/or gel filtration steps.

GST Pull-Down Assay

15 μ g GST fusion protein in 30 μ l GST pull-down buffer (50 mM Tris-HCl [pH 8.0], 200 mM NaCl, 10 mM b-ME, 0.1% Tween 20) was incubated with 20 μ g glutathione Sepharose resin (QIAGEN) for 1 hr. Then the target protein (20 μ g in 120 μ l GST pull-down buffer) was added to the resin. After 1-hr incubation with rotation, the resin was washed three times, and the protein was eluted with 15 μ l 2 \times SDS loading buffer at 95°C for 5 min. The eluted proteins were resolved by 10% SDS-PAGE and visualized by Coomassie blue staining.

Crosslinking Mass Spectrometry Analysis

45 μ l purified protein complex (4.5 mg/ml for Tpz1-Ccq1; 4 mg/ml for Tpz1-Poz1; 1.25 mg/ml for Tpz1-Pot1) was mixed with 5 μ l DSSO (dissolved in DMSO) to the final concentration as indicated in results. Crosslinking was performed for 30 min and quenched with 2 μ l 1 M Tris-HCl (pH 8.0) for 15 min. The cysteine residues were reduced with 4 mM TCEP and alkylated with 20 mM iodoacetamide in dark, followed by terminating alkylation reaction with 20 mM cysteine for 30 min. The crosslinked proteins were digested overnight at 37°C with trypsin (2%, w/w) and chymotrypsin (5%, w/w), separately. Crosslinked peptides were analyzed by LC MSⁿ utilizing an LTQ-Orbitrap XL MS (Thermo Fisher Scientific) coupled online with an Easy-nLC 1000 (Thermo Fisher Scientific) as described (Kao et al., 2011). Each MSⁿ experiment consists of one MS scan in FT mode (350–1,400 m/z, resolution of 60,000 at m/z 400) followed by two data-dependent MS² scans in FT mode (resolution of 7,500) with normalized collision energy at 20% on the top two MS peaks with charges 3⁺ or up, and three MS³ scans in the LTQ with normalized collision energy at 35% on the top three peaks from each MS².

Identification of DSSO Crosslinked Peptides by LC-MSⁿ

MS3 data were subjected to a developmental version of Protein Prospector (v.5.10.10) for database searching, using Batch-Tag with mass tolerances for parent ions and fragment ions set as ± 20 ppm and 0.6 Da, respectively. Trypsin was set as the enzyme with five maximum missed cleavages allowed. A maximum of five variable modifications were also allowed, including protein N-terminal acetylation, methionine oxidation, N-terminal conversion of glutamine to pyroglutamic acid, asparagine deamidation, and cysteine carbamidomethylation. In addition, three defined modifications on uncleaved lysines and free protein N termini were also selected: alkene (A: C₃H₂O, +54 Da); sulfenic acid (S: C₃H₄O₂S, +104 Da), and unsaturated thiol (T: C₃H₂OS, +86 Da) modifications, due to remnant moieties of DSSO. Initial acceptance criteria for peptide identification required a reported expectation value ≤ 0.1 .

Integration of MSⁿ data was carried out using the in-house program Link-Hunter, a revised version of the previously written Link-Finder program, to validate and summarize crosslinked peptides as previously described (Kao et al., 2011, 2012).

Co-immunoprecipitation

The indicated strains were grown in YEAU and harvested at OD₆₀₀ = 0.6–0.8. Then the cell pellets were cryogenically disrupted with FastPrep MP with two pulses (60 s) of bead-beating in ice-cold lysis buffer (50 mM HEPES [pH 7.5], 140 mM NaCl, 15 mM EGTA, 15 mM MgCl₂, 0.1% NP40, 0.5 mM Na₃VO₄, 1 mM NaF, 2 mM PMSF, 2 mM benzamidine, Complete proteinase inhibitor

[Roche]). The crude extracts were clarified by centrifuge for 10 min and adjusted to 15 mg/ml. Anti-Flag M2 affinity gel (Sigma) or anti-Myc resin (9E10, Santa Cruz Biotechnology) was equilibrated with same lysis buffer, and immunoprecipitation was performed for 3 hr at 4°C. Then, the proteins were eluted with 30 μ l 0.1 M glycine (pH 2.0) at room temperature for 10 min with gentle shaking and neutralized by Tris-HCl (pH 8.0) immediately after elution. Eluted proteins were resolved by 8% SDS-PAGE and then subjected to western blotting. Western blot analysis was performed using monoclonal anti-Flag (M2-F1804, from Sigma), monoclonal anti-Myc (9E10, from Covance), monoclonal anti-HA (F-7, from Santa Cruz), anti-Ccq1 rabbit serum, and anti-Cdc2 (γ 100.4, from Abcam). 20 μ g whole-cell extract was used for input control.

Telomere Length Analysis

S. pombe cells grown in 5 ml YEAU overnight were harvest for genomic DNA extraction. EcoRI-digested genomic DNA was separated on 1% agarose gel and then transferred to N⁺ membrane (GE Healthcare) via capillary blot. The telomeric probe was prepared as previously described (Jun et al., 2013). The template of *pol1*⁺ was amplified with 5' primer (GGTGCAGAAGACGGTCTG CAAG) and 3' primer (CTTAGCATGCAGAAGCATGCGC), and the *pol1*⁺ probe was generated by High Prime (Roche). Southern blots were imaged using a Bio-Rad phosphorimager.

In Vitro Translation Coupled with GST Pull-Down Assay

hPOT1 in a pET28 vector was mutated by site-directed mutagenesis PCR. WT and all mutants were in vitro expressed using TnT coupled reticulocyte lysate kit (Promega) following the manual. Briefly, a 25- μ l reaction containing 20 μ l rabbit reticulocyte lysate, 0.5 μ g plasmid, 1 μ l 1mM methionine, and 1 μ l [³⁵S]methionine was incubated at 30°C for 90 min. 22 μ l of each in vitro translation reaction was directly applied to GST pull-down assay as previously described, but with 7 μ g of GST fusion protein. The pull-downs were resolved by 8% SDS-PAGE and imaged with a Bio-Rad phosphorimager.

Electrophoretic Mobility Shift Assay

20 nM 5' end ³²P-labeled ssDNA (GTTACGGTTACAGGTTACG) was mixed with Pot1 proteins of specified concentrations in 20 μ l reaction buffer (20 mM Tris-HCl [pH 8.0], 100 mM NaCl, 5 mM DTT, 2 mM MgCl₂, 10% glycerol). The mixtures were then incubated at 4°C for 30 min. The protein-ssDNA complex were resolved by 7% non-denaturing polyacrylamide gel and imaged with a Bio-Rad phosphorimager.

Chromatin Immunoprecipitation

Fresh *S. pombe* cells in liquid culture were fixed with an 11% formaldehyde solution (11% formaldehyde, 100 mM NaCl, 1 mM EDTA [pH 8.0], 0.5 mM EGTA, 50 mM Tris-HCl [pH 8.0]) for 20 min, followed by termination with 125 mM glycine for 5 min. Cell pellets were disrupted in 400 μ l of lysis buffer (50 mM HEPES [pH 7.5], 140 mM NaCl, 1 mM EDTA, 1% Triton X-100, 0.1% sodium deoxycholate, complete proteinase inhibitor [Roche], 1 mM PMSF, 1 mM benzamide, 1 mM Na₂VO₄, 1 mM NaF) with FastPrep MP. After three pulses (1 min) of beads-beating, at least 90% cells were broken. Cell extracts were sonicated three times for 30 s in 18 cycles using a Bioruptor. Clarified cell extracts were incubated with anti-Myc resin (9E10, Santa Cruz) or anti-Ccq1 rabbit serum followed by protein G-agarose (Roche) for 3 hr at 4°C. Then, the beads were washed twice with lysis buffer, lysis buffer with 500 mM NaCl, wash buffer, and 1 \times TE buffer sequentially. Each sample was added with 100 μ l of 10% Chelex100 resin and boiled for 15 min, followed by 20 μ g proteinase K treatment for 30 min at 55°C. The recovered DNA were denatured with 0.4 M NaOH and transferred to a Hybond-XL membrane by using a slot module. The blots were hybridized with telomeric probe; the same blot was then re-probed with rDNA probe after stripping.

SUPPLEMENTAL INFORMATION

Supplemental Information includes five figures and one table and can be found with this article online at <http://dx.doi.org/10.1016/j.celrep.2015.08.043>.

AUTHOR CONTRIBUTIONS

J.L. performed biochemical and molecular genetics experiments. C.Y. performed LC-MSⁿ analyses with supervision from L.H. X.H. performed ChIP experiments. J.-K.K. prepared some recombinant proteins, participated in benchmarking of MICro-MS, and made protein structure figures. J.C.B. participated in the initial stage of the project and made some Ccq1 mutant constructs/strains. H.-I.J. aided in telomere length analysis. S.D.R. provided chemical reagent DSSO. F.Q. conceived the project. F.Q., L.H., J.L., and C.Y. designed the experimental plans. F.Q. and J.L. wrote the manuscript with L.H. and C.Y. writing the mass spectrometry part.

ACKNOWLEDGMENTS

We thank Toru Nakamura, Fuyuki Ishikawa, Julie Cooper, Virginia Zakian, and Takashi Toda for providing plasmids and strains, and Peter Kaiser, Craig Kaplan, and Songtao Jia for comments on the manuscript and helpful discussions. This work was supported by a Basil O'Connor Starter Scholar Research Award from March of Dimes, a Beginning Grant-in-Aid from American Heart Association, NIH grants R01GM098943 to F.Q., as well as R01GM074830 to L.H. and R01GM106003 to L.H. and S.D.R. H.-I.J. is supported by a Predoctoral Fellowship (15PRE22420012) from the American Heart Association.

Received: April 22, 2015

Revised: July 12, 2015

Accepted: August 11, 2015

Published: September 10, 2015

REFERENCES

- Aoude, L.G., Pritchard, A.L., Robles-Espinoza, C.D., Wadt, K., Harland, M., Choi, J., Gartside, M., Quesada, V., Johansson, P., Palmer, J.M., et al. (2015). Nonsense mutations in the shelterin complex genes ACD and TERF2IP in familial melanoma. *J. Natl. Cancer Inst.* 107, 107.
- Armstrong, C.A., Pearson, S.R., Amelina, H., Moiseeva, V., and Tomita, K. (2014). Telomerase activation after recruitment in fission yeast. *Curr. Biol.* 24, 2006–2011.
- Artandi, S.E., and Cooper, J.P. (2009). Reverse transcribing the code for chromosome stability. *Mol. Cell* 36, 715–719.
- Bähler, J., Wu, J.Q., Longtine, M.S., Shah, N.G., McKenzie, A., 3rd, Steever, A.B., Wach, A., Philippsen, P., and Pringle, J.R. (1998). Heterologous modules for efficient and versatile PCR-based gene targeting in *Schizosaccharomyces pombe*. *Yeast* 14, 943–951.
- Baumann, P., and Cech, T.R. (2001). Pot1, the putative telomere end-binding protein in fission yeast and humans. *Science* 292, 1171–1175.
- Borah, S., Xi, L., Zaug, A.J., Powell, N.M., Dancik, G.M., Cohen, S.B., Costello, J.C., Theodorescu, D., and Cech, T.R. (2015). TERT promoter mutations and telomerase reactivation in urothelial cancer. *Science* 347, 1006–1010.
- Cooper, J.P., Nimmo, E.R., Allshire, R.C., and Cech, T.R. (1997). Regulation of telomere length and function by a Myb-domain protein in fission yeast. *Nature* 385, 744–747.
- de Lange, T. (2005). Shelterin: the protein complex that shapes and safeguards human telomeres. *Genes Dev.* 19, 2100–2110.
- Erzberger, J.P., Stengel, F., Pellarin, R., Zhang, S., Schaefer, T., Aylett, C.H., Cimerancic, P., Boehringer, D., Sali, A., Aebersold, R., and Ban, N. (2014). Molecular architecture of the 40S-eIF1-eIF3 translation initiation complex. *Cell* 158, 1123–1135.
- Günes, C., and Rudolph, K.L. (2013). The role of telomeres in stem cells and cancer. *Cell* 152, 390–393.
- Hanahan, D., and Weinberg, R.A. (2011). Hallmarks of cancer: the next generation. *Cell* 144, 646–674.

- Horn, S., Figl, A., Rachakonda, P.S., Fischer, C., Sucker, A., Gast, A., Kadel, S., Moll, I., Nagore, E., Hemminki, K., et al. (2013). TERT promoter mutations in familial and sporadic melanoma. *Science* 339, 959–961.
- Horvath, M.P., Schweiker, V.L., Bevilacqua, J.M., Ruggles, J.A., and Schultz, S.C. (1998). Crystal structure of the *Oxytricha nova* telomere end binding protein complexed with single strand DNA. *Cell* 95, 963–974.
- Houghtaling, B.R., Cuttonaro, L., Chang, W., and Smith, S. (2004). A dynamic molecular link between the telomere length regulator TRF1 and the chromosome end protector TRF2. *Curr. Biol.* 14, 1621–1631.
- Huang, F.W., Hodis, E., Xu, M.J., Kryukov, G.V., Chin, L., and Garraway, L.A. (2013). Highly recurrent TERT promoter mutations in human melanoma. *Science* 339, 957–959.
- Jain, D., and Cooper, J.P. (2010). Telomeric strategies: means to an end. *Annu. Rev. Genet.* 44, 243–269.
- Jun, H.I., Liu, J., Jeong, H., Kim, J.K., and Qiao, F. (2013). Tpz1 controls a telomerase-nonextendible telomeric state and coordinates switching to an extendible state via Ccq1. *Genes Dev.* 27, 1917–1931.
- Kaake, R.M., Wang, X., Burke, A., Yu, C., Kandur, W., Yang, Y., Novitsky, E.J., Second, T., Duan, J., Kao, A., et al. (2014). A new in vivo cross-linking mass spectrometry platform to define protein-protein interactions in living cells. *Mol. Cell. Proteomics* 13, 3533–3543.
- Kao, A., Chiu, C.L., Vellucci, D., Yang, Y., Patel, V.R., Guan, S., Randall, A., Baldi, P., Rychnovsky, S.D., and Huang, L. (2011). Development of a novel cross-linking strategy for fast and accurate identification of cross-linked peptides of protein complexes. *Mol. Cell. Proteomics* 10, <http://dx.doi.org/10.1074/mcp.M110.002212>.
- Kao, A., Randall, A., Yang, Y., Patel, V.R., Kandur, W., Guan, S., Rychnovsky, S.D., Baldi, P., and Huang, L. (2012). Mapping the structural topology of the yeast 19S proteasomal regulatory particle using chemical cross-linking and probabilistic modeling. *Mol. Cell. Proteomics* 11, 1566–1577.
- Leitner, A., Joachimiak, L.A., Unverdorben, P., Walzthoeni, T., Frydman, J., Förster, F., and Aebersold, R. (2014). Chemical cross-linking/mass spectrometry targeting acidic residues in proteins and protein complexes. *Proc. Natl. Acad. Sci. USA* 111, 9455–9460.
- Liu, D., Safari, A., O'Connor, M.S., Chan, D.W., Laegeler, A., Qin, J., and Songyang, Z. (2004). PTOP interacts with POT1 and regulates its localization to telomeres. *Nat. Cell Biol.* 6, 673–680.
- Loayza, D., and De Lange, T. (2003). POT1 as a terminal transducer of TRF1 telomere length control. *Nature* 423, 1013–1018.
- Marks, D.S., Colwell, L.J., Sheridan, R., Hopf, T.A., Pagnani, A., Zecchina, R., and Sander, C. (2011). Protein 3D structure computed from evolutionary sequence variation. *PLoS ONE* 6, e28766.
- Miyoshi, T., Kanoh, J., Saito, M., and Ishikawa, F. (2008). Fission yeast Pot1-Tpp1 protects telomeres and regulates telomere length. *Science* 320, 1341–1344.
- Ovchinnikov, S., Kamisetty, H., and Baker, D. (2014). Robust and accurate prediction of residue-residue interactions across protein interfaces using evolutionary information. *eLife* 3, e02030.
- Palm, W., and de Lange, T. (2008). How shelterin protects mammalian telomeres. *Annu. Rev. Genet.* 42, 301–334.
- Pathare, G.R., Nagy, I., Śledź, P., Anderson, D.J., Zhou, H.J., Pardon, E., Steyaert, J., Förster, F., Bracher, A., and Baumeister, W. (2014). Crystal structure of the proteasomal deubiquitylation module Rpn8-Rpn11. *Proc. Natl. Acad. Sci. USA* 111, 2984–2989.
- Politis, A., Stengel, F., Hall, Z., Hernández, H., Leitner, A., Walzthoeni, T., Robinson, C.V., and Aebersold, R. (2014). A mass spectrometry-based hybrid method for structural modeling of protein complexes. *Nat. Methods* 11, 403–406.
- Ramsay, A.J., Quesada, V., Foronda, M., Conde, L., Martínez-Trillos, A., Villamor, N., Rodríguez, D., Kwarciak, A., Garabaya, C., Gallardo, M., et al. (2013). POT1 mutations cause telomere dysfunction in chronic lymphocytic leukemia. *Nat. Genet.* 45, 526–530.
- Robles-Espinoza, C.D., Harland, M., Ramsay, A.J., Aoude, L.G., Quesada, V., Ding, Z., Pooley, K.A., Pritchard, A.L., Tiffen, J.C., Petljak, M., et al. (2014). POT1 loss-of-function variants predispose to familial melanoma. *Nat. Genet.* 46, 478–481.
- Sato, M., Dhut, S., and Toda, T. (2005). New drug-resistant cassettes for gene disruption and epitope tagging in *Schizosaccharomyces pombe*. *Yeast* 22, 583–591.
- Sexton, A.N., Regalado, S.G., Lai, C.S., Cost, G.J., O'Neil, C.M., Urnov, F.D., Gregory, P.D., Jaenisch, R., Collins, K., and Hockemeyer, D. (2014). Genetic and molecular identification of three human TPP1 functions in telomerase action: recruitment, activation, and homeostasis set point regulation. *Genes Dev.* 28, 1885–1899.
- Shi, J., Yang, X.R., Ballew, B., Rotunno, M., Calista, D., Fargnoli, M.C., Ghorzo, P., Bressac-de Paillerets, B., Nagore, E., Avril, M.F., et al.; NCI DCEG Cancer Sequencing Working Group; NCI DCEG Cancer Genomics Research Laboratory; French Familial Melanoma Study Group (2014). Rare missense variants in POT1 predispose to familial cutaneous malignant melanoma. *Nat. Genet.* 46, 482–486.
- Speedy, H.E., Di Bernardo, M.C., Sava, G.P., Dyer, M.J., Holroyd, A., Wang, Y., Sunter, N.J., Mansouri, L., Juliusson, G., Smedby, K.E., et al. (2014). A genome-wide association study identifies multiple susceptibility loci for chronic lymphocytic leukemia. *Nat. Genet.* 46, 56–60.
- Sugiyama, T., Cam, H.P., Sugiyama, R., Noma, K., Zofall, M., Kobayashi, R., and Grewal, S.I.S. (2007). SHREC, an effector complex for heterochromatic transcriptional silencing. *Cell* 128, 491–504.
- Taboski, M.A., Sealey, D.C., Dorrens, J., Tayade, C., Betts, D.H., and Harrington, L. (2012). Long telomeres bypass the requirement for telomere maintenance in human tumorigenesis. *Cell Rep.* 1, 91–98.
- Tadeo, X., Wang, J., Kallgren, S.P., Liu, J., Reddy, B.D., Qiao, F., and Jia, S. (2013). Elimination of shelterin components bypasses RNAi for pericentric heterochromatin assembly. *Genes Dev.* 27, 2489–2499.
- Takai, K.K., Kibe, T., Donigian, J.R., Frescas, D., and de Lange, T. (2011). Telomere protection by TPP1/POT1 requires tethering to TIN2. *Mol. Cell* 44, 647–659.
- Velázquez-Muriel, J., Lasker, K., Russel, D., Phillips, J., Webb, B.M., Schneidman-Duhovny, D., and Sali, A. (2012). Assembly of macromolecular complexes by satisfaction of spatial restraints from electron microscopy images. *Proc. Natl. Acad. Sci. USA* 109, 18821–18826.
- Walzthoeni, T., Leitner, A., Stengel, F., and Aebersold, R. (2013). Mass spectrometry supported determination of protein complex structure. *Curr. Opin. Struct. Biol.* 23, 252–260.
- Wang, F., Podell, E.R., Zaugg, A.J., Yang, Y., Baciú, P., Cech, T.R., and Lei, M. (2007). The POT1-TPP1 telomere complex is a telomerase processivity factor. *Nature* 445, 506–510.
- Webb, C.J., and Zakian, V.A. (2012). *Schizosaccharomyces pombe* Ccq1 and TER1 bind the 14-3-3-like domain of Est1, which promotes and stabilizes telomerase-telomere association. *Genes Dev.* 26, 82–91.
- Weigt, M., White, R.A., Szurmant, H., Hoch, J.A., and Hwa, T. (2009). Identification of direct residue contacts in protein-protein interaction by message passing. *Proc. Natl. Acad. Sci. USA* 106, 67–72.
- Worden, E.J., Padovani, C., and Martin, A. (2014). Structure of the Rpn11-Rpn8 dimer reveals mechanisms of substrate deubiquitination during proteasomal degradation. *Nat. Struct. Mol. Biol.* 21, 220–227.
- Yang, B., Wu, Y.J., Zhu, M., Fan, S.B., Lin, J., Zhang, K., Li, S., Chi, H., Li, Y.X., Chen, H.F., et al. (2012). Identification of cross-linked peptides from complex samples. *Nat. Methods* 9, 904–906.
- Ye, J.Z., Hockemeyer, D., Krutchinsky, A.N., Loayza, D., Hooper, S.M., Chait, B.T., and de Lange, T. (2004). POT1-interacting protein PIP1: a telomere length regulator that recruits POT1 to the TIN2/TRF1 complex. *Genes Dev.* 18, 1649–1654.

Cell Reports

Supplemental Information

**Dissecting Fission Yeast Shelterin
Interactions via MICro-MS Links Disruption
of Shelterin Bridge to Tumorigenesis**

Jinqiang Liu, Clinton Yu, Xichan Hu, Jin-Kwang Kim, Jan C. Bierma, Hyun-Ik Jun, Scott D. Rychnovsky, Lan Huang, and Feng Qiao

Figure S1

A

Rpn8



S. cerevisiae 1 -----MSLQHEKVTIAPLVLLSAIDHYERTQT-KENKRCVGVILGDNSSSTIRVT
C. albicans 1 MSTTATSTNELALLDKSVVVSPLVLLSVVDHYNRVAK-DSKRRVVGVLGDNSTDTIKVT
A. oryzae 1 --MPATTADTLSLVTRTVTVAPLVLLSVADHYGRSAK-GTRKRVVGVLGDNSSGQNVRS
S. pombe 1 -MPPAVSSETSTIVPQQVIVHPLVLLSAVDSYNRSKAK-GTKRRVVGILLGQNNGDVVNVVA
H. sapiens 1 -----MPELAVQKVVVHPLVLLSVVDHENRICKVGNQKRVVGVLGDSWQKKVLDVS

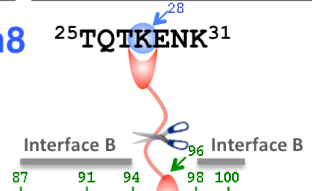
Interface B
S. cerevisiae 50 NSFALPFEDEKNSDVWFLDHNFIENMNECKKINAKEKLIIGWYHSGPKLRASDLKINEL
C. albicans 60 NSFALPFEDEKNSDVWFLDHNFIIDSMGEMFKKINAKEKLIIGWYHSGPKLRASDLKINEL
A. oryzae 58 NSFALPFEDEKNSDVWFLDHNFIIVSMRDMFKKINAREKLIIGWYHSGPKLRASDLKINEL
S. pombe 59 NSFALPFEDEKNSDVWFLDHNFIIVSMNEMFKKINANEKLIIGWYHSGPKLRASDLKINEL
H. sapiens 52 NSFALPFEDEKNSDVWFLDHNFIIVSMYGMFKKINAREKLIIGWYHSGPKLRASDLKINEL

B

Rpn11

S. cerevisiae 24 KETVYISSLALLKMLKHGRAGVPMELVMGLMLGEFVDDYTVNVVDFVAMPQSGTGVSVEAVD
C. albicans 30 SETVYISSLALLKMLKHGRAGVPMELVMGLMLGEFVDDYTHVHDFVAMPQSGTGVSVEAVD
A. oryzae 32 SETVYISSLALLKMLKHGRAGVPMELVMGLMLGEFVDDYTVRVVDFVAMPQSGTGVSVEAVD
S. pombe 27 SECVYISSLALLKMLKHGRAGVPMELVMGLMLGEFVDDYTVRVVDFVAMPQSGTGVSVEAVD
H. sapiens 28 AECVYISSLALLKMLKHGRAGVPMELVMGLMLGEFVDDYTVRVVDFVAMPQSGTGVSVEAVD

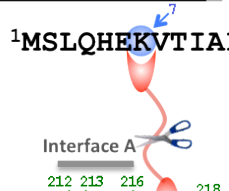
Rpn8



S. cerevisiae 85 DVFOAKMMDMLKQTRGRPEMVGWYHSHPGFGCWLSSVDINTQQSFEQLNSRAVAVVVDPIQ
C. albicans 91 DVFOAKMMDMLKQTRGRPEMVGWYHSHPGFGCWLSSVDINTQQSFEQLNKRVAVAVVVDPIQ
A. oryzae 93 PVFOAKMMDMLKQTRGRPEMVGWYHSHPGFGCWLSSVDINTQQSFEQLTPRAVAVVVDPIQ
S. pombe 88 PVFOAKMMDMLKQTRGRPEMVGWYHSHPGFGCWLSSVDINTQQSFEQLTPRAVAVVVDPIQ
H. sapiens 89 PVFOAKMMDMLKQTRGRPEMVGWYHSHPGFGCWLSSVDINTQQSFEQLNSRAVAVVVDPIQ

S. cerevisiae 146 SVKGKVVDAFRLIDTGALNNLEPRQTTSNLGLLNKANIQALIHGLNRHYYSINIDYHKT
C. albicans 152 SVKGKVVDAFRLIDTTTLNMGQEPROSTSNVGHNLKPSIQALIHGLNRHYYSINIDYHKT
A. oryzae 154 SVKGKVVDAFRLIQPQTVVMGQEPROTTSNLGHNLKPSIQALIHGLNRHYYSINIDYHKT
S. pombe 149 SVKGKVVDAFRLINPSTLNMGQEPROTTSNLGHNLKPSIQALIHGLNRHYYSINIDYHKT
H. sapiens 150 SVKGKVVDAFRLINANMVIIGHEPRQTTSNLGHNLKPSIQALIHGLNRHYYSINIDYHKT

Rpn8



S. cerevisiae 207 AKETKMLNMLNLHKEQ
C. albicans 213 EYETNMLNMLNLHKKN
A. oryzae 215 GLEENMLNMLNLHKEV
S. pombe 210 ELEEMMLNMLNLHKKQ
H. sapiens 211 ELEQKMLNMLNLHKKK

Figure S2

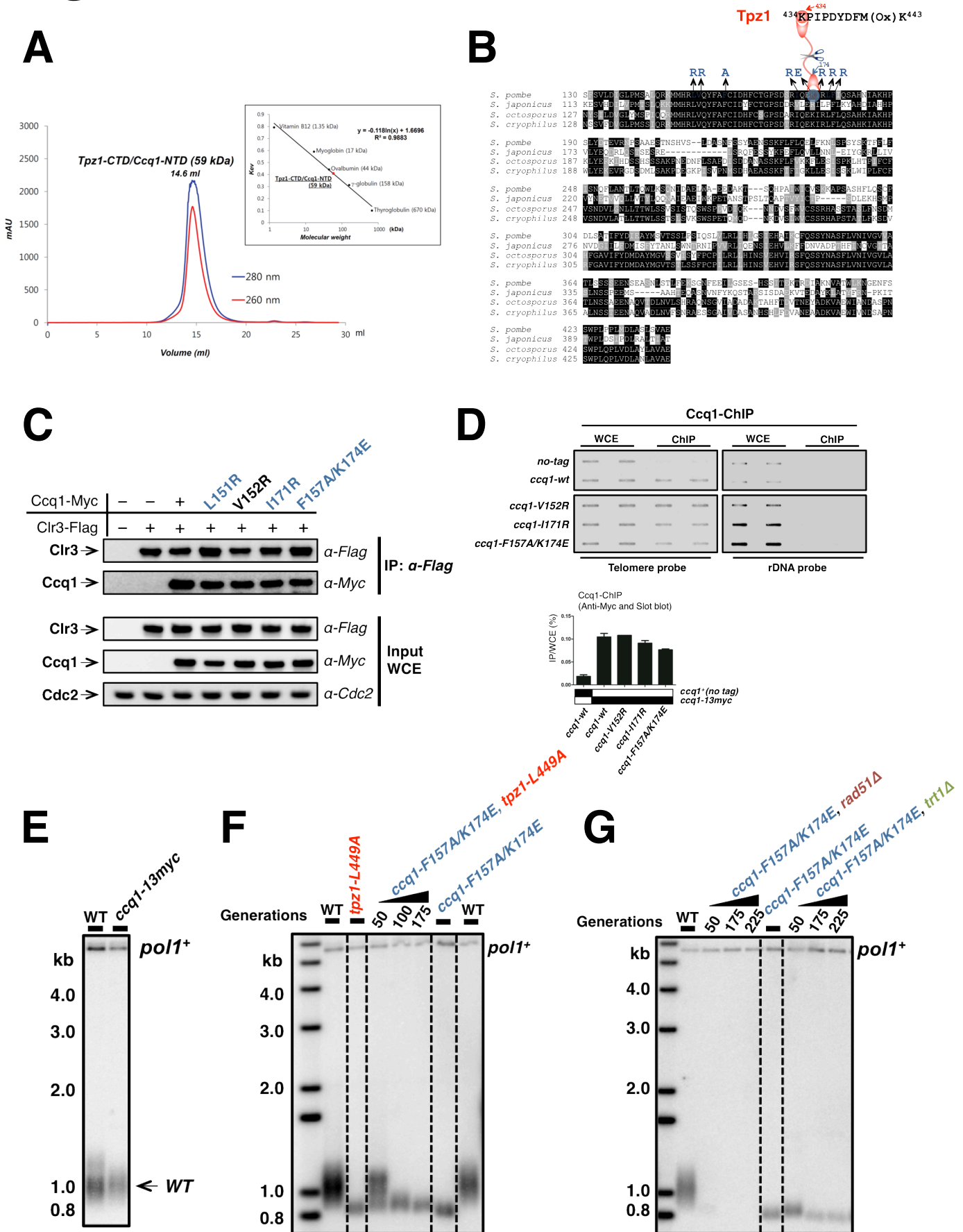
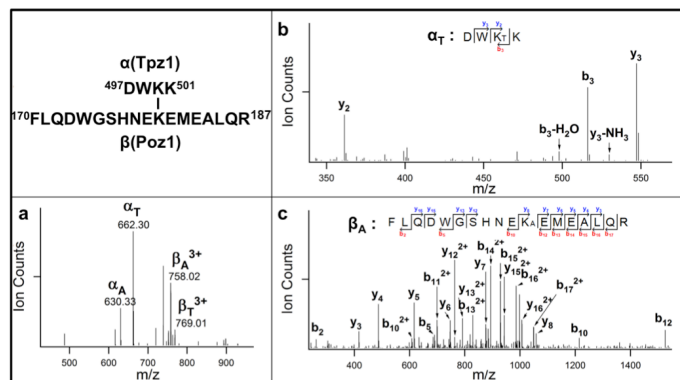


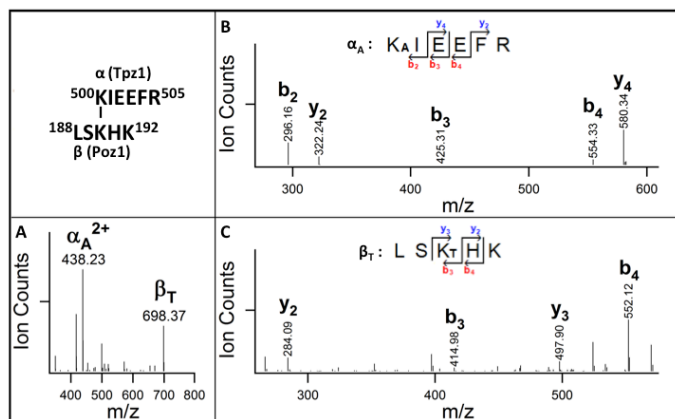
Figure S3

A



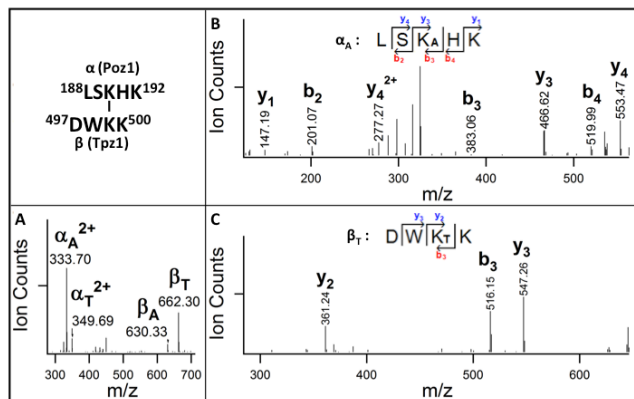
MSⁿ analysis identifies a linkage between residue K180 of Poz1 and K499 of Tpz1.

C



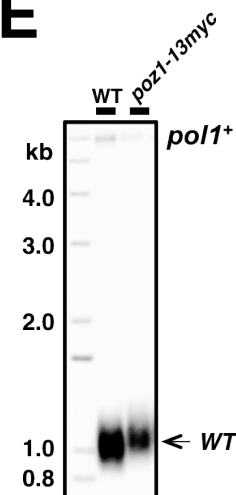
MSⁿ analysis identifies a linkage between residue K190 of Poz1 and K500 of Tpz1.

B



MSⁿ analysis identifies a linkage between residue K190 of Poz1 and K499 of Tpz1.

E



D

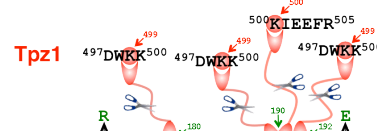
Poz1

```

S. pombe      1  -MNEKIRSQSVLNLETFEKENHDMQRESSIVACLRYLGYSKSCHEKPIIFM
S. japonicus 1  MHKIEQKAALITVAILEYLLRSKQEKSAQAHAGQBAFVEYLGHLPLGLETKKPIIFV
S. octosporus 1  -MIHHSQAAATFKSLEAFFLSENHFQFTSENAAIVQACLENLGTCSLEYVPIIFM
S. cryophilus 1  -MHHSQAAATLKSLEAFFLSENHFQFTSENAAIVQACLENLGTCSLEYVPIIFM

S. pombe      57  DIAFIEYCFNLSLPSFQNPITQTQPPDSCQILWYSLISNALERLENIEERQNC
S. japonicus  58  SPAFISYCFNIEGFHGRGSKEDASKP--IACFWDDTVMNSALFQLKTEHSRKKR
S. octosporus 57  NIAFIDCFALKVR--TIPDMNEDLNLTSQAILWDTDLISRSLHILACTEERLEC
S. cryophilus 57  NIAFIDCFALKVRS--TIPSMNDSNLTLSQAILWDTDLISRSLHILSYIENERTEC

S. pombe      114  MREDGLVRYTNEPLLNETLNNEAKLYSCAKAGICRWMAFHELEQEPIDHINEFK
S. japonicus  113  ILKILR--DLDEFTVRLRSIDKEAMRIAAKAGICRWMLFSTIKERVDEEAVLA
S. octosporus 112  FRSLSLSSLNKNDERYARECNLDEAKLYVVAKTGIIRWMSFHLLEQRQVDFSAISK
S. cryophilus 112  EHLSTSSNKNDDERLACEINLDAEAKLYAVAKTGILRWMLFHLLEQRVLDLKSFS
    
```



```

S. pombe      170  FLQDWGSHNEKEMALQRLSKHKIRKLIYVSOHKKKMPSEKNSWLSRYIQCTKIQ
S. japonicus  169  FLTMMMDVPEIQTFKRLISYDWDHRSKIKYKPKKIPWSKMYSMORYLACTEAQ
S. octosporus 169  FLDWYVDNPESEKKVLEKIASLYEDKRFQKQVFSQMPWVKIHSILGRYLLCTKLE
S. cryophilus 169  FLDWYVDSSNEKKVLEKITLDEKRTQKILHFQSEMPWVKIHSILGRYLLCTKLE

S. pombe      227  LEFCDYDFKQREIKMLTSNIN-----
S. japonicus  226  CKLVNQPCFADTFLAAVEAIEQNQRVLSIFSGNGI
S. octosporus 226  LELEFHGYNL-----
S. cryophilus 226  LELEFHGYNFQSKTILFF-----
    
```

Figure S4

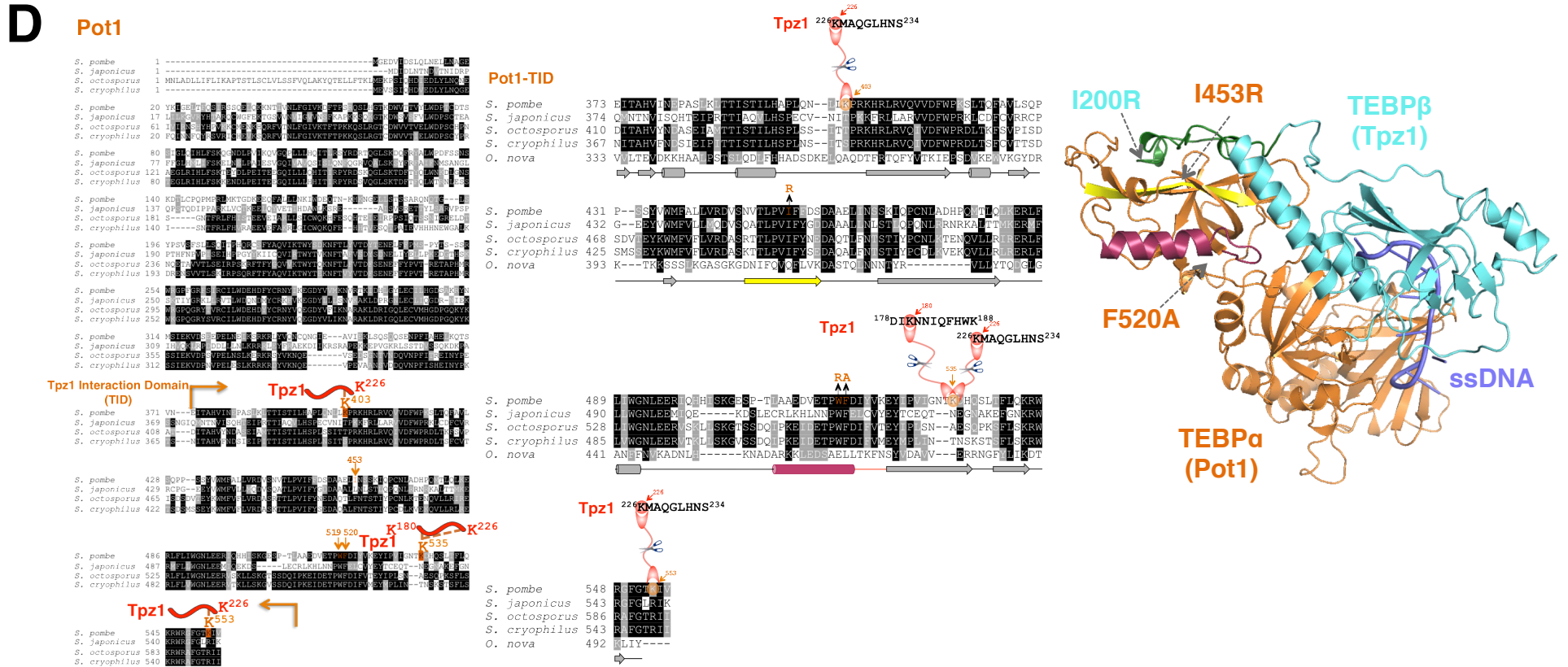
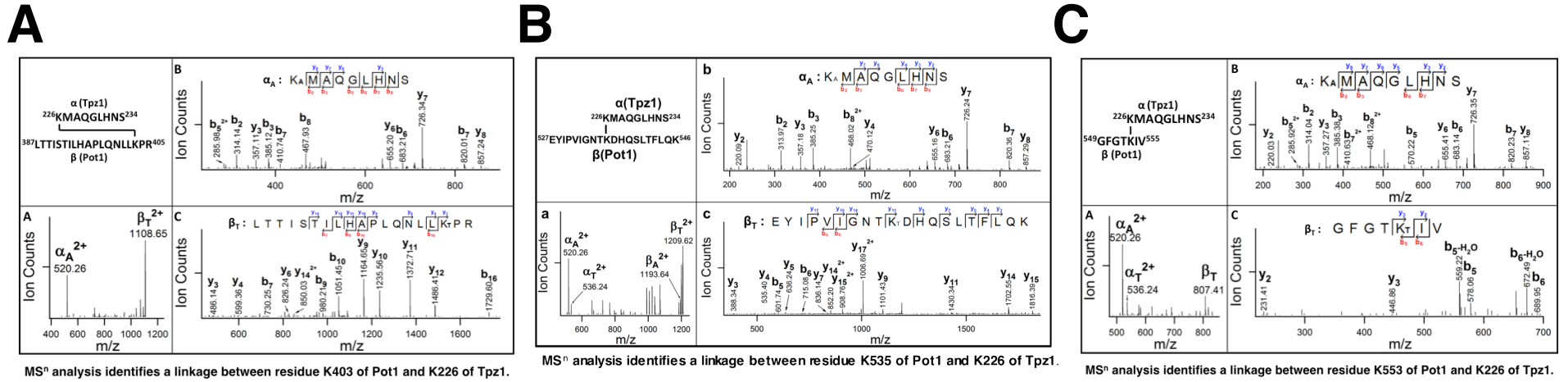
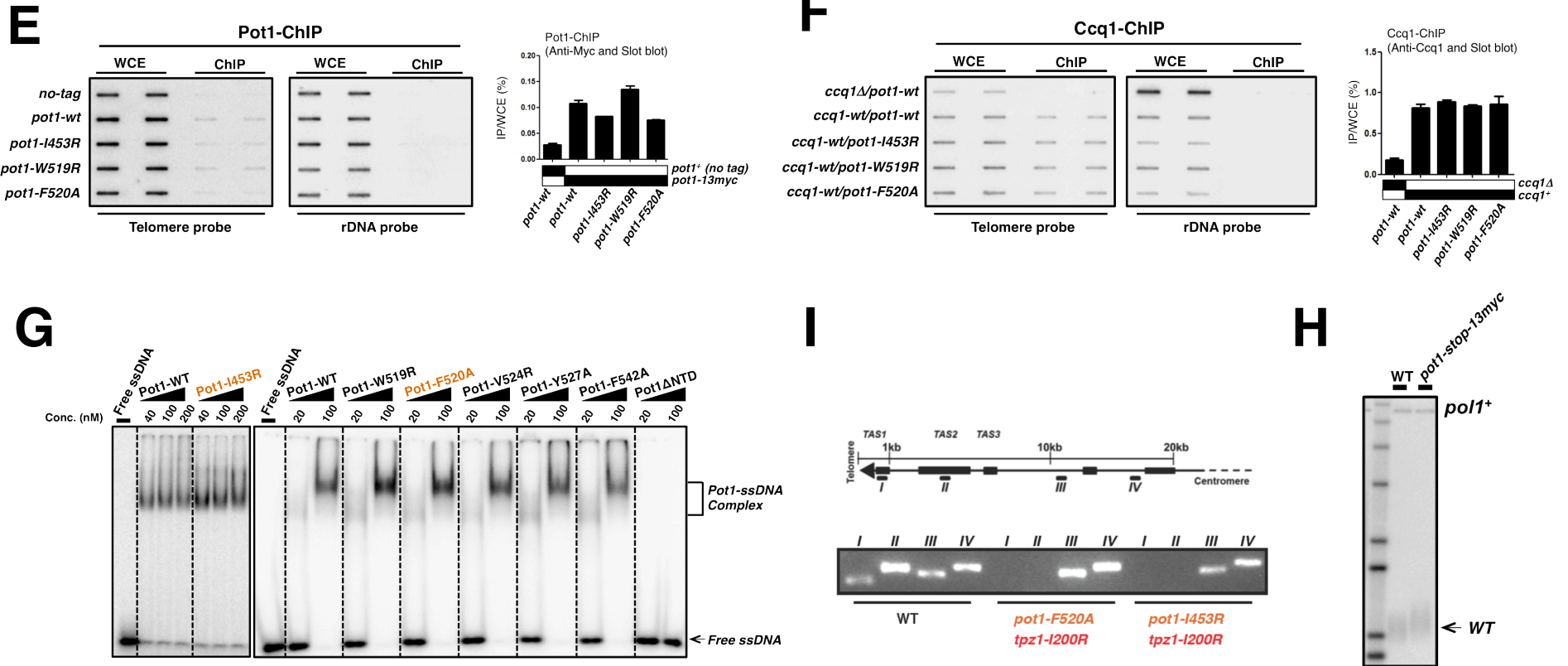


Figure S4



Supplementary Figure Legends

Figure S1. (Related to Figure 2)

Sequence alignments of Rpn8 (A) and Rpn11 (B) from fungi to human. Identical residues are highlighted in black, and chemically similar residues are highlighted in gray. The crosslinked lysine residues are highlighted in blue and green for Rpn8 and Rpn11, respectively. Crosslinked peptides are shown on the top with crosslinked lysines indicated. The residues colored in blue or green with residue numbers above are the contact residues observed in the interface from the crystal structure from Rpn8 and Rpn11, respectively. In sequence alignment of Rpn11 (B), Zn²⁺-coordinating residues are colored in blue and residues involved in catalysis are in red.

Figure S2. (Related to Figure 3)

(A) Gel filtration chromatography showing Tpz1-CTD and Ccq1-NTD complex forms a dimer of the Tpz1-CTD/Ccq1-NTD heterodimer.

(B) Sequence alignment of Ccq1 from four different fission yeast species. The crosslinked lysine is highlighted in dark blue with corresponding Tpz1 fragment on the top. The targeted residues for mutation are colored in dark blue and were mutated to the amino acids indicated above them.

(C) Co-immunoprecipitation (co-IP) assays evaluating the binding between Clr3 and Ccq1 mutants. The mutants colored in dark blue are Tpz1-binding deficient. Cdc2 was shown as the loading control. Input: 1/30 of input WCE (whole cell extract).

(D) Localization of Ccq1 mutants to telomere is monitored by ChIP assay. Slot-blot was used to visualize telomeric association of Ccq1 in each genetic background. Telomeric enrichment of Ccq1 was expressed as immunoprecipitate (IP)/whole-cell extract (WCE) from the telomere DNA probe hybridization. The same membrane was stripped and then hybridized with the rDNA probe. Error bars in the quantitation of the slot blot analysis represent standard deviations of two individual repeats.

(E) *ccq1-wt-13myc* has wild-type telomere length. Therefore, C-terminal tagging of *ccq1*⁺ does not interfere with telomere maintenance.

(F) *ccq1-F157A/K174E tpz1-L449A* double-mutant cells have identical telomere phenotype as either *ccq1-F157A/K174E* or *tpz1-L449A* cells.

(G) Telomere maintenance in *ccq1-F157A/K174E* cells is not telomerase dependent, but HR dependent.

Figure S3. (Related to Figure 4)

- (A) MSⁿ analysis of a DSSO crosslinked peptide representing an interaction between Poz1 and Tpz1.
- (a) MS² spectrum of a quadruply-charged crosslinked peptide α - β (m/z 739.5940⁴⁺) in which two characteristic peptide fragment pairs were detected: α_T/β_A (m/z 662.30⁺/758.02³⁺) and α_A/β_T (m/z 630.33⁺/769.01³⁺) with defined modifications. Respective MS³ spectra of (b) α_T (m/z 662.30⁺) and (c) β_A (m/z 758.02³⁺) fragment ions unambiguously identified their sequences as DWK_TK of Tpz1 and FLQDWGSHNEK_AEMEALQR of Poz1. This identifies a linkage between residue K180 of Poz1 and K499 of Tpz1.
- (B) MSⁿ analysis of a DSSO crosslinked peptide representing an interaction between Poz1 and Tpz1.
- (a) MS² analysis of a triply-charged parent ion α - β (m/z 449.2354³⁺) in which two characteristic peptide fragment pairs were detected: α_A/β_T (m/z 333.70²⁺/662.30¹⁺) and α_T/β_A (m/z 349.69²⁺/630.33¹⁺), unique to DSSO inter-linked peptides; MS³ spectra of (b) α_A (m/z 333.70²⁺) and (c) β_T (m/z 662.30¹⁺) fragment ions detected in (a), which unambiguously identify their sequences as LSK_AHK of Poz1 and DWK_TK of Tpz1, respectively. This identifies a linkage between residue K190 of Poz1 and K499 of Tpz1. Note: K_A: alkene modified lysine; K_T: unsaturated thiol modified lysine.
- (C) MSⁿ analysis of a DSSO crosslinked peptide representing an interaction between Poz1 and Tpz1.
- (a) MS² spectrum of a triply-charged parent ion α - β (m/z 530.9461³⁺), in which a characteristic peptide fragment pair was detected: α_A/β_T (m/z 438.23²⁺/698.37¹⁺), unique to DSSO inter-linked peptides; MS³ spectra of (b) α_A (m/z 438.23²⁺) and (c) β_T (m/z 698.37¹⁺) fragment ions detected in (a), which unambiguously identified their sequences as K_AIEEFR of Tpz1 and LSK_THK of Poz1, respectively, indicating a linkage between residue K190 of Poz1 and K500 of Tpz1. Note: K_A: alkene modified lysine; K_T: unsaturated thiol modified lysine.
- (D) Sequence alignment of Poz1 from four different fission yeast species. The crosslinked lysines are highlighted in dark blue with corresponding Tpz1 peptide fragments on the top. The targeted residues for mutation are colored in green and were mutated to the amino acids indicated above them.
- (E) *poz1-wt-13myc* has wild-type telomere length. Therefore, C-terminal tagging of *poz1*⁺ does not interfere with telomere maintenance.

Figure S4. (Related to Figure 5)

- (A) MSⁿ analysis of a DSSO crosslinked representing an interaction between Pot1 and Tpz1. (a) MS² spectrum of a triply-charged parent ion α - β (m/z 818.7060⁴⁺), in which a characteristic peptide fragment pair was detected: α_A/β_T (m/z 520.26²⁺/1108.65²⁺), unique to DSSO inter-linked peptides; MS³ spectra of (b) α_A (m/z 520.26²⁺) and (c) β_T (m/z 1108.65²⁺) fragment ions detected in (a), which

unambiguously identified their sequences as K_AMAQGLHNS of Tpz1 and LTTISTILHAPLQNLLK_TPR of Pot1, respectively, indicating a linkage between residue K403 of Pot1 and K226 of Tpz1. Note: K_A: alkene modified lysine; K_T: unsaturated thiol modified lysine.

(B) MSⁿ analysis of a DSSO crosslinked peptide representing an interaction between Pot1 and Tpz1.

(a) MS² spectrum of a quadruply-charged crosslinked parent ion α - β (m/z 869.196⁴⁺), in which two characteristic peptide fragment pairs were detected: α_A/β_T (m/z 520.26²⁺/1209.62²⁺) and α_T/β_A (m/z 536.24²⁺/1193.64²⁺), unique to DSSO inter-linked peptides. MS³ spectra of (b) α_A (m/z 520.26²⁺) and (c) β_T (m/z 1209.62²⁺) fragment ions unambiguously identified their sequences as K_AMAQGLHNS of Tpz1 and EYIPVIGNTK_TTDHQSFLTFLQK of Pot1, respectively, indicating a linkage between residues K535 of Pot1 and K226 of Tpz1.

(C) MSⁿ analysis of a DSSO crosslinked peptide representing an interaction between Pot1 and Tpz1.

(a) MS² spectrum of the triply-charged parent ion α - β (m/z 621.9794³⁺) in which three characteristic peptide fragments were detected: α_A/β_T (m/z 520.26²⁺/807.41¹⁺) and α_T (m/z 536.24²⁺), unique to DSSO inter-linked peptides; MS³ spectra of (b) α_A (m/z 520.26²⁺) and (c) β_T (m/z 807.41¹⁺) fragment ions detected in (a), which unambiguously identified their sequences as K_AMAQGLHNS of Tpz1 and GFGTK_TIV of Pot1 respectively. This demonstrates a linkage between residue K553 of Pot1 and K226 of Tpz1. Note: K_A: alkene modified lysine; K_T: unsaturated thiol modified lysine.

(D) Left: Sequence alignment of Pot1 from four different fission yeast species. The crosslinked lysines are highlighted in light brown with the corresponding Tpz1 fragment (colored in red) shown on the top. The crosslinked lysines all fall in the Tpz1-interacting region, which is indicated by two arrows colored in light brown. **Middle:** An enlarged view of the Tpz1-interacting region of Pot1. The selected residues of Pot1 for mutation are colored in light brown and mutated to the amino acids indicated above them.

Right: Structural representation of *Oxytricha nova* TEBP α /TEBP β complex, an ortholog of Tpz1/Pot1 complex. The loop region of TEBP β that mediates protein-protein interaction between TEBP- α and - β is colored green and the location of a previously identified Tpz1 mutant I200R that disrupts Tpz1-Pot1 interaction is indicated. The locations two Pot1 mutants (I453R and F520A) identified in this study, based on sequence alignment, are also indicated by arrows. The structural elements in which I453R and F520A reside in are color yellow and dark red, respectively.

(E) Telomere localization of Pot1 mutants is monitored by ChIP assay. Slot-blot was used to quantitate telomeric association of Pot1 in each genetic background. Error bars in the quantitation of the slot-blot represent standard deviations of two individual repeats.

(F) Telomere localization of Ccq1 to telomere is monitored by ChIP assay in Pot1 mutant strains. Slot-blot was used to visualize telomere association of Ccq1 in each Pot1 mutant background. Error bars in

the quantitation of the slot-blot analysis represent standard deviations of two individual repeats.

(G) Gel-shift experiments evaluating the binding ability of Pot1 mutants to a ^{32}P -labeled telomeric ssDNA. The position of unbound telomeric ssDNA in the gel is indicated by an arrow. The Tpz1-binding defective mutants are colored in light brown. Pot1 Δ NTD is a Pot1 truncation variant without N-terminal OB1-OB2 domains, serving as a negative control.

(H) *pot1-wt-stop-13myc* has wild-type telomere length. Therefore, selection cassette insertion does not affect telomere maintenance.

(I) **Upper:** Schematic diagram of chromosome showing sub-telomeric regions. Greek numbers indicate the locations where the PCR primers are designed. **Lower:** *pot1-F520A/tpz1-I200R* and *pot1-I453R/tpz1-I200R* mutants lost sub-telomeric I and II regions. The PCR products (from I to IV) are amplified from corresponded regions on chromosomes (upper diagram). For *pombe* cells carrying circular chromosomes due to telomere deprotection, both sub-telomeric regions I and II are eroded from chromosome ends.

Figure S5. (Related to Figure 6)

Sequence alignment of Pot1 from fission yeast to different vertebrates. The *S. pombe* Pot1 and human POT1 are highlighted in grey. Tpz1-interacting region is indicated by two arrows. In the sequence alignment, the Tpz1-binding defective mutant of *S. pombe* Pot1-I453R (colored in light brown) resides in the corresponding region of human POT1-A532P identified in familial melanoma patients (highlighted in red box).